

**Investigation of the Importance of Cumulus Convection and
Ventilation in Early Tropical Storm Development**

by
Raúl Erlando López

Technical Paper No. 124
Department of Atmospheric Science
Colorado State University
Fort Collins, Colorado



**Department of
Atmospheric Science**

Paper No. 124

INVESTIGATION OF THE IMPORTANCE OF
CUMULUS CONVECTION AND VENTILATION IN EARLY
TROPICAL STORM DEVELOPMENT

by

Raúl Erlando López

This report was prepared with support from

NSF GF-287
ESSA E-22-80-68(G)

Department of Atmospheric Science
Colorado State University
Fort Collins, Colorado

June 1968

Atmospheric Science Paper No. 124

TABLE OF CONTENTS

	Page
ABSTRACT	iii
INTRODUCTION	1
DATA SOURCES AND ANALYSIS METHODS	4
Objective Analysis Scheme	5
COMPARATIVE DESCRIPTION OF BOTH CASES	8
Synoptic History	8
Flow Characteristics	9
Moisture and Temperature Patterns	10
Convergence Patterns	11
Satellite Information	12
Radar Information	13
DEVELOPMENT REQUIREMENTS	41
QUANTITATIVE ASSESSMENT OF DISTURBANCE	
HEATING PROCESSES	48
Heat Sources	50
Sub-cloud convergence	50
Convergence above cloud base	63
Heat Sinks	65
Ventilation	65
Divergent outflow at upper levels	68
Computation of Net Warming	69
CONCLUSIONS AND FINAL REMARKS	79
ACKNOWLEDGMENTS	83
REFERENCES	84

ABSTRACT

Two well documented cases of tradewind disturbances are studied. One disturbance developed into hurricane Carla (1961) while the other failed to intensify. Initially the two cases appeared to be very similar but on closer inspection the flow patterns in which the disturbances were embedded proved to have significant differences. This paper describes these differences.

The thermodynamics of development is investigated with a simple hydrostatic model to obtain an estimate, from actual data, of the magnitudes and interrelationships of the factors controlling the accumulation and concentration of heat. Computations of tropospheric heating are performed in 12 hour steps. In the developing disturbance the warming due to low-level moisture convergence was twice as large as in the non-developing case. On the other hand, the cooling from ventilation was three times smaller, and the cooling resulting from middle level convergence was also much less for this case. This furnished the developing case with a mechanism for accumulation of latent heat four or five times larger than the non-developing disturbance.

The net warming resulting from latent heat release in the developing case was, however, too small to account for all of the observed pressure falls at the surface. When the effect of the cumulus convection was carefully examined, it was found that only 10 percent of the latent heat contained in the low-level moisture convergence (surface to 950 mb) was available to raise the enthalpy of the disturbance. Part of the latent heat is lost as the moist air mixes with the environment in shallow convection. Another part is used for expansion and potential energy increase. Of the remaining portion, only that part which gives the cloud air an excess enthalpy above the disturbance's enthalpy can be used to warm the system. This warming is insufficient to fully account for vortex intensification. In the light of these results the role of the cumulus clouds as the primary heat source in early disturbance intensification should be reexamined. Consideration should be given to the influence of additional warming resulting from the trapping of infrared radiation under the cloud canopies.

I INTRODUCTION

Understanding the development of hurricanes is a very challenging endeavor. Their relative rarity and extreme violence has aroused the curiosity of many investigators. Despite much interest, the structure of disturbances in the tradewinds and the processes that modify those disturbances into hurricanes are not well understood.

There is little general agreement among tropical meteorologists as to the precise environmental requirements and processes that lead to tropical storm development. Some investigators envision hurricanes as resulting from the intensification of wave-like perturbations of the tradewinds (Riehl, 1948a, 1948b, 1950; Yanai, 1961; Fett, 1966), while others look for intensification mechanisms associated with the Equatorial Trough (Sadler, 1963; Tanabe, 1963). The postulated requirements for development are likewise varied.

The primary reason for the difficulty in obtaining a consistent development theory has been lack of observational data. The observational networks in the tropics have always been deficient. Another reason is the lack of understanding of the role played by cumulus convection, and of an integrated view that incorporates the role of the planetary boundary layer in the coupling of lower and upper level broad-scale flows.

With the advent of special instrumented aircraft flights and the weather satellite, the observational potentialities have been greatly improved. More observational studies are needed in light of this new data in order to clarify the physical processes which lead to intensification.

In this study an observational description of the structure of two disturbances in the tradewinds of the Caribbean Sea, and the development mechanisms acting on them, will be presented. In addition a simple physical model is developed to incorporate the different mechanisms which act to produce and accumulate heat. An accumulation of heat is necessary to achieve a reduction of the surface pressure. In order to determine the tropospheric heating in both cases, computations of the net disturbance warming are performed in 12 hour steps.

One of the disturbances developed into hurricane Carla (1961). The other traveled along the same path two weeks earlier without intensifying. These were the first cases of early disturbance development and non-development for which National Hurricane Research Laboratory instrumented aircraft and satellite information were simultaneously available within the best tropical data network of the world, the West Indies.

The disturbance that gave rise to hurricane Carla has been the subject of studies by Alaka (1963) and Fett (1964). They have concentrated their investigations on the later stages of

development while this study is concerned with the earliest stages of the disturbance. Krishnamurti and Baumhefner (1966) have applied a numerical analysis scheme to the non-developing disturbance of 13 August 1961.

This study differs from these and other investigations in that consideration is not given to the detailed flow dynamics. We are concerned only with the processes which lead to production and accumulation of heat within the disturbance relative to its environment.

II DATA SOURCES AND ANALYSIS METHODS

For the synoptic analysis, use was made of an objective analysis program of the West Indies region prepared by Yanai (1964). This analysis directly averages the observations by using a bilinear interpolation formula. It was free of the usual balance assumptions of numerical models. This objective analysis scheme was used to remove the subjective factors of hand interpolations. However, synoptic data and charts were also obtained from the Miami and San Juan Weather Bureau Offices for comparison with the machine objective analyses.

The instrumented research aircraft of the National Hurricane Research Laboratory provided wind, temperature, and pressure measurements every one to two seconds at selective flight levels. Photographs of the airborne PPI radar scope gave information on the cumulus clouds and rainfall distribution for approximately 100 miles around the aircraft's position. From these radar pictures composite diagrams of the radar cloud information were drawn. Hawkins, et. al. (1962) has given information concerning the instrumentation of the aircraft data. These aircraft observations provided meso-scale and microscale information which the synoptic information cannot give.

The satellite data was in the form of computer produced maps of equivalent black body temperatures obtained from infrared radiation measurements of TIROS III channel 2. The data

consisted of grid point values from individual radiation measurements which were sampled by the computer every 0.13 seconds along the viewing scan of the radiometer.

Objective Analysis Scheme

The objective analysis program for the Caribbean region prepared by Yanai (op. cit.) basically consists of an iterative correction procedure. The process starts with actual data. A best guess is made at every grid point. Successive corrections are applied on the estimated grid values until a reasonable agreement is achieved between observations and estimated values at the stations. The initial analyzed maps are used as a first guess for the next analysis period.

Assume that we have one of the iterative estimates at all grid points. Consider four adjacent points. These points will define a square inside of which actual stations may be located. Using a bilinear interpolation formula the four adjacent grid points are used to compute an interpolated value at each one of the actual stations inside the grid square defined by the four points. The difference between the actual value and the interpolated estimate will be used to give a correction to the four adjacent grid points. For a given grid point the application of the "combined" corrections of all the stations in a specific neighborhood of the point will give the next iterative estimate. The combination of the corrections is

accomplished using an exponential weighting factor according to the distance of the station from the grid point.

The grid spacing of the objective analysis was 4° and the area analyzed covered the regions $12-40^\circ$ North Latitude and $60-100^\circ$ West Longitude. Fig. 7 shows the typical analysis. To insure good fit at the boundaries input data was accepted 12° beyond the boundaries. The height interval between individual levels was 100 mb except at lowest levels where the surface and 975 mb levels were used. The highest level of analysis was 125 mb.

The objective analysis was applied to the wind fields at all levels and also to the surface pressure field. Computations were made consecutively from the surface to 125 mb. The average of the lower level and the corresponding previous time period was used as the first guess of the next adjacent upper level. From the objectively analyzed wind data, additional computations of divergence, vorticity and vertical motion were performed. All available data was included.¹ The objective analyses agreed very well with the hand analyses. There were only isolated points where the calculated speeds appeared to be larger than expected. These non-representative values occurred only in data-void areas where sharp surrounding speed gradients were present. Great care was

¹Data from the Cuban upper air stations of Havana and Camaguey were still available for the time periods of the two cases studied.

exercised in rejecting or modifying these anomalous and erroneous values. These slight difficulties are inherent in most objective analysis schemes. They did not significantly affect the computations of this study. For a more detailed description of the iterative method and smoothing procedure the reader is referred to Yanai's (op. cit.) original report.

III COMPARATIVE DESCRIPTION OF BOTH CASES

At first inspection the two cases appeared to be very similar. Both disturbances moved through the same region just two weeks apart (Fig. 1). Initially they appeared to be of equal intensity (Figs. 9 and 11). Time cross-sections for Grand Cayman (Figs. 2 and 3) and Kingston (Figs. 4 and 5) indicate that both disturbances had troughs with strong cyclonic wind shifts at low-levels. The upper tropospheric flow patterns (Figs. 7 and 10) were also much alike. In addition, the research aircraft motion pictures of the clouds showed very similar heavy overcast sky conditions. Closer inspection, however, indicated that there were important fundamental differences between the two cases in their intensification potential.

Synoptic History

The disturbance from which Carla developed was detected by satellite as early as August 31 (Fig. 14a) to the east of the Lesser Antilles. It is probable that it existed much earlier as an easterly perturbation along the Equatorial Trough off the West African Coast. The disturbance moved across the Caribbean and slowly intensified into a tropical depression. By 1000Z, 5 September it had attained tropical storm strength. The storm continued a slow and steady intensification (Fig. 6) attaining hurricane strength early on the 6th. In contrast, the mid-August disturbance traveled along the same route but did not develop a closed circulation.

Flow Characteristics

The 200 mb maps for the developing case are shown in Figs. 7a-e. Most of the flow features at this level persisted throughout the period of early development. These upper flow characteristics were typical of the usual flow features experienced during tropical storm development as have been observed by a number of researchers, particularly Colón and Nightingale (1963). Equatorwards of 14° N easterly winds were present at 200 mb. As shown in the N-S cross-section of zonal wind along 64° W. of Fig. 8, cyclonic horizontal shearing conditions were present at low levels. Frictional veering in the planetary boundary layer would lead to forced surface convergence in this horizontal shearing region. Figs. 9a-e show the 700 mb level progression of the wave. The southern part of the disturbance, where most of the convective activity was found, was located in an area of surface horizontal shearing flow underneath weak 200 mb easterly flow. Prior to its intensification, the developing case was thus located in an area of small tropospheric vertical shear and large low-level cyclonic horizontal shear.

Figs. 10a-c and Figs. 11a-e show the 200 and 700 mb broad-scale flow patterns for the non-developing disturbance. On first inspection the broad-scale features of these flow conditions appeared to be similar to those of the development case. The position of the disturbance relative to the upper-level anticyclone, the strong

wind shift at the trough line to the west and the presence of cyclonic horizontal wind shear at low-levels were all very similar. Nevertheless, significantly different vertical shearing conditions were observed. A large westerly wind component was found at upper levels over the non-developing disturbance area during the latter stages of its movement across the Caribbean. This lead to larger tropospheric vertical wind shear and to a greater advection or "ventilation" of heat away from the non-developing disturbance. This was an important inhibiting feature.

Moisture and Temperature Patterns

Figs. 2 and 3 show time cross-sections of temperature and relative humidity anomalies at Grand Cayman for the non-developing disturbance. Figs. 4 and 5 are the corresponding time cross-sections at Kingston for the developing case. To the east of the disturbance axis and above the 700 mb level the relative humidities for both cases are very high. To the west of the wave axis the relative humidities are very low. This follows the usual observed concentration of convective activity and moisture in the region of highest cyclonic vorticity advection to the east of the trough axis as first described by Riehl (1945).

The temperature anomalies likewise indicate warming (between 500 and 200 mb) east of the axes in both disturbances. The non-developing disturbance shows marked cooling at upper levels

ahead of the axis, while the developing case shows warming both ahead and behind the trough axis.

Above the warmer temperature anomalies at levels between 100 and 200 mb, the development case had negative temperature anomalies. This is indicative that a greater density of deep cumulus convection was present in the development case. The upper tropospheric lapse rates of the tropics require that cumulus penetration to the tropopause (~ 100 mb) induce negative temperature anomalies above 200 mb.

Convergence Patterns

The development case low-level convergence maps show that the maximum values of this parameter are not strong ($\sim 5 \times 10^{-6} \text{ sec}^{-1}$).² Low-level convergence was concentrated at the southern end of the disturbance. The average vertical distribution of the convergence in a 3° radius around the center during the two days of 3 and 4 September is shown in Fig. 12. Maximum convergence is located at 975 mb. A secondary maximum is present at 700 mb where the flow curvature is strongest.

The non-developing case surface maps also portray a weak maximum of convergence at the southern end of the disturbance.

²Low-level convergence was calculated in two ways, from Yanai's objective analysis and then from a direct, individual composite of all land and sea observations at each time period. Both independent calculations gave about the same results. The latter calculations were used in the computations of low-level moisture inflow.

The two day mean vertical profile of divergence for this case is pictured in Fig. 13. Two levels of maximum convergence are again present at 975 and 650 mb. The 650 mb convergence is, however, considerably larger than at low-levels. Compared to the developing disturbance the non-developing case had stronger convergence at middle levels and weaker convergence at lower levels. Krishnamurti and Baumhefner (1966) also observed large middle level convergence for this non-developing case.

Satellite Information

The radiation data of channel two from the TIROS III satellite was available for a number of time periods during the life history of the developing and non-developing cases. Figs. 14a-c show the development case equivalent black body temperature in degrees Kelvin (first figure of 2 omitted) as seen by the satellite's infrared radiometers. Figs. 15a-c portray the same features for the non-developing case.

The general satellite observed cloud configurations agree well with the wave position and wind field as determined from synoptic analyses. The low-level convergence computed from the objective analyses matches surprisingly well the general cloud features seen from the satellite. The satellite pictures demonstrate the organized nature and conservatism of the cloud-blob patterns in association with both disturbances and their typical size scale. Many other satellite studies have verified this typical 'cloud blob' association.

Radar Information

The radar composites of the cumulus rainfall echoes in Figs. 16-19 are also closely correlated with the satellite cloud data and the convergence fields from the objective wind analyses. The radar cumulus cloud composite of the very early development stage on 4 September (Fig. 16) shows many more intense rain echoes than the radar composites of the non-developing disturbance (Figs. 18 and 19). The larger but slightly fainter echoes of the non-development case may be indicative of middle-level clouds and a weaker surface convergence. The development case thus possessed a much greater amount of cumulus convection.

In summary, the major observational differences between the early stages of the development and non-development case were:

- 1) the development case had approximately twice as much low-level convergence and a larger amount of cumulus convection associated with it
- 2) the non-development case had much greater middle level convergence
- 3) the tropospheric vertical wind shears in the later periods of the non-development case were larger

In most other observational features the two cases were very similar.

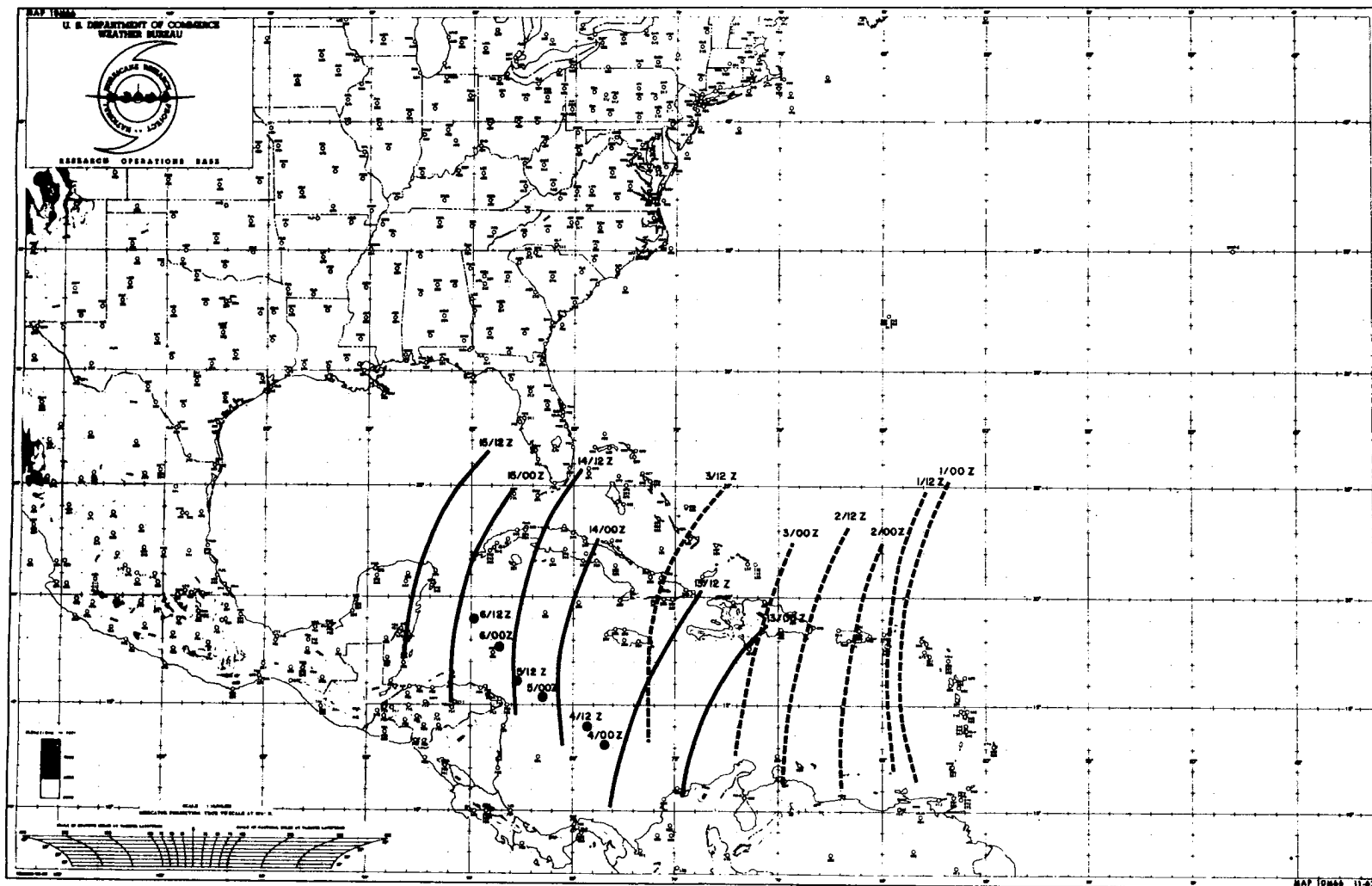


Fig. 1. Sequential position of the axes and centers of the cases studied. Solid lines correspond to the non-developing case, August, 1961. Dashed lines correspond to developing disturbance, September, 1961. Solid dots show vortex positions of developing case.

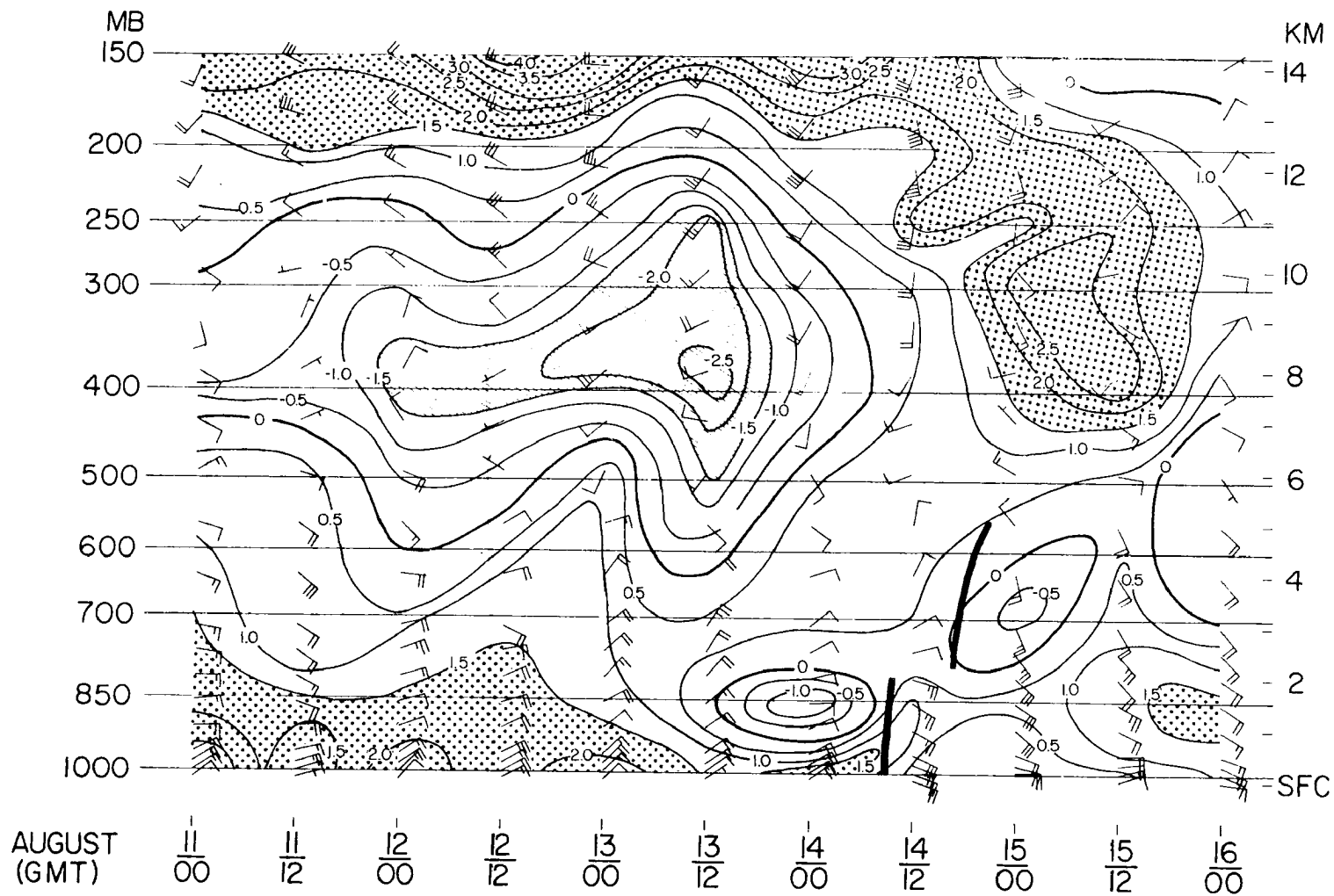


Fig. 2. Cross-section of wind (in knots) and temperature anomaly ($^{\circ}$ C) from the mean summertime tropical atmosphere for Grand Cayman, August 11-16 (non-developing case). Heavy solid line indicates the trough of the disturbance.

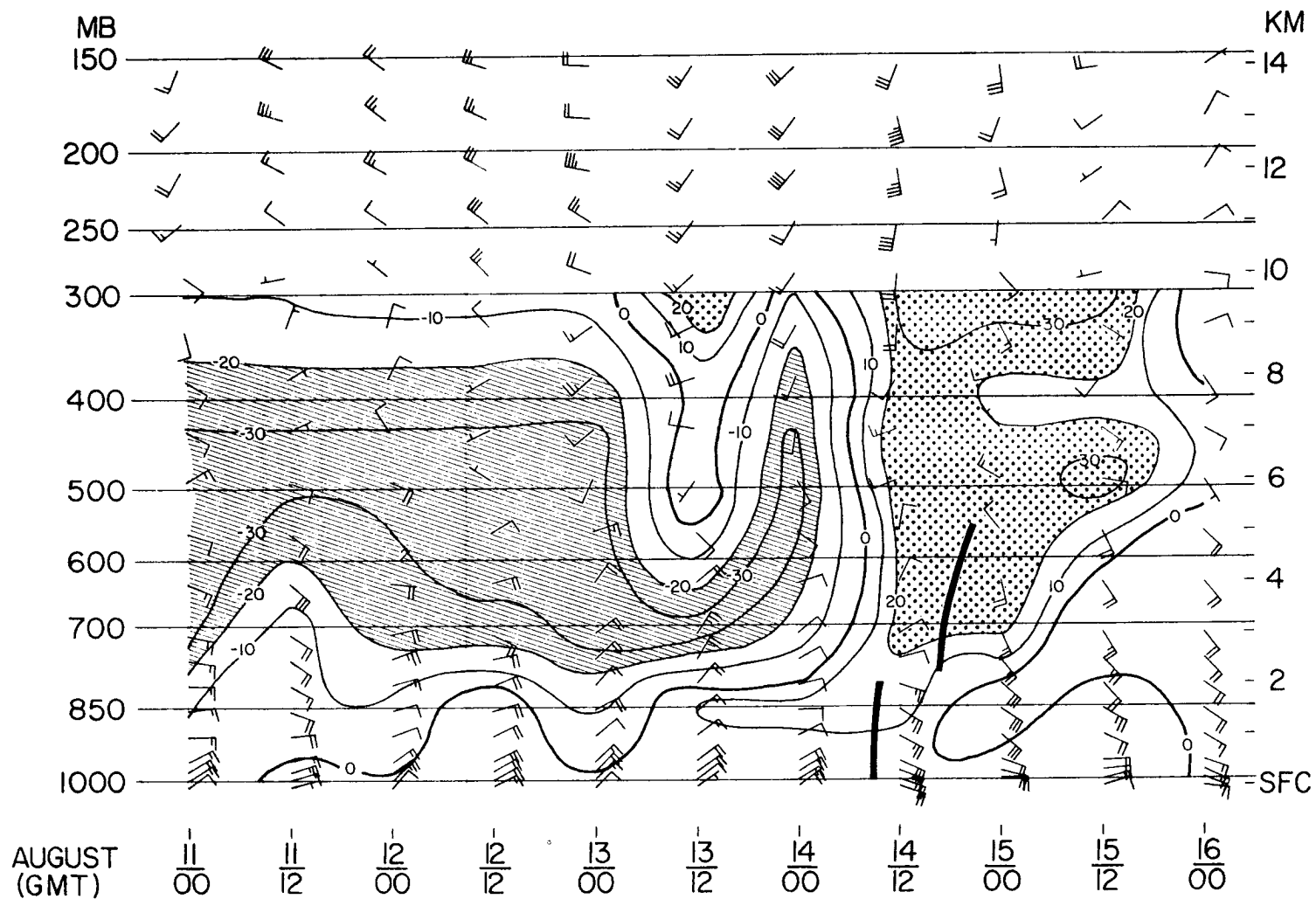


Fig. 3 Cross-section of wind (in knots) and relative humidity anomaly from the mean tropical atmosphere for Grand Cayman, August 11-16, 1961 (non-developing case). Heavy solid line indicates the trough of the disturbance.

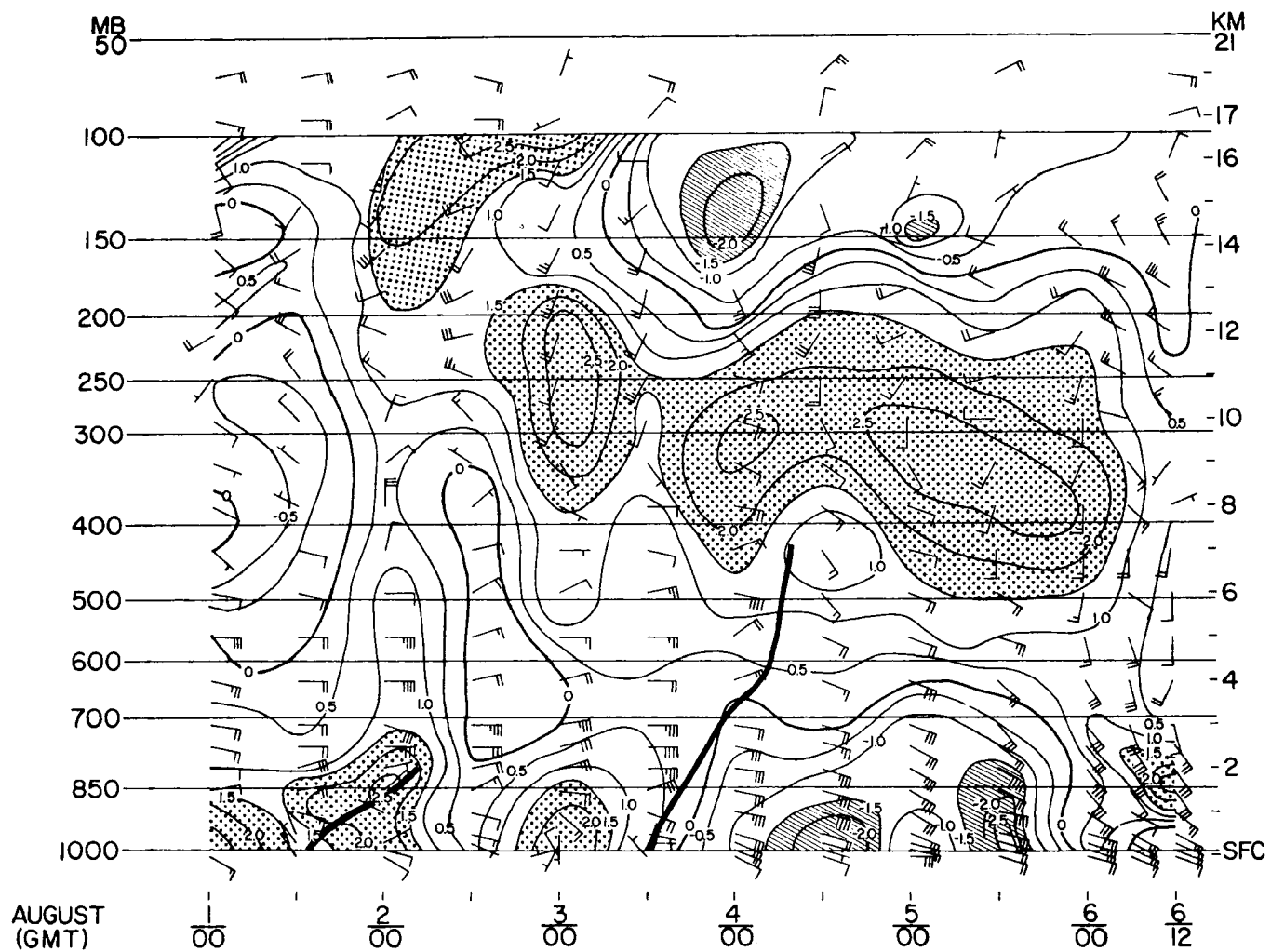


Fig. 4. Cross-section of wind (in knots) and temperature anomaly ($^{\circ}\text{C}$) from the mean summertime tropical atmosphere for Kingston, September 2-7, 1961 (development case). Heavy solid line indicates the trough of the disturbance.

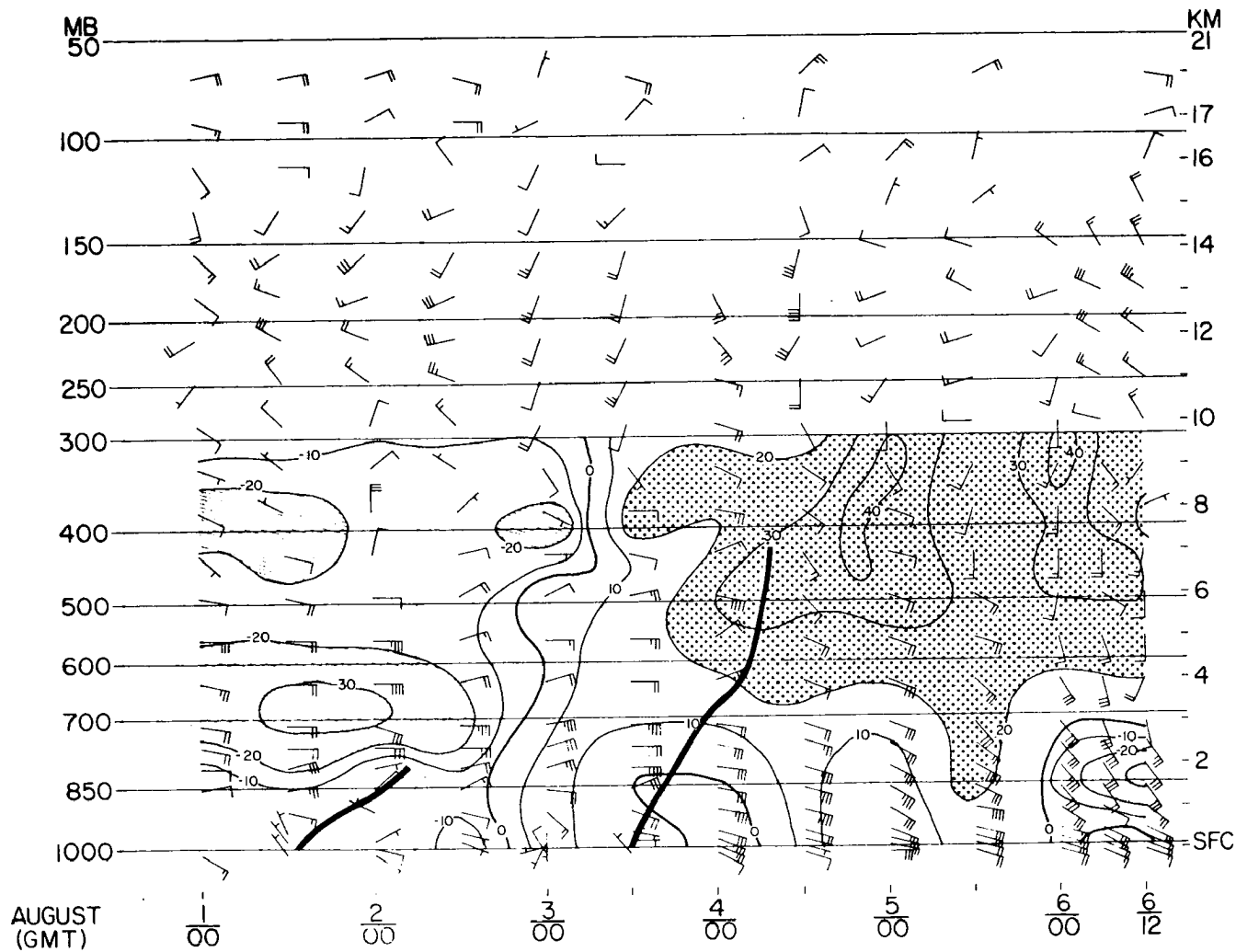


Fig. 5. Cross-section of wind (in knots) and relative humidity anomaly from the mean tropical atmosphere for Kingston. September 2-7, 1961 (development case). Heavy solid line indicates the trough of the disturbance.

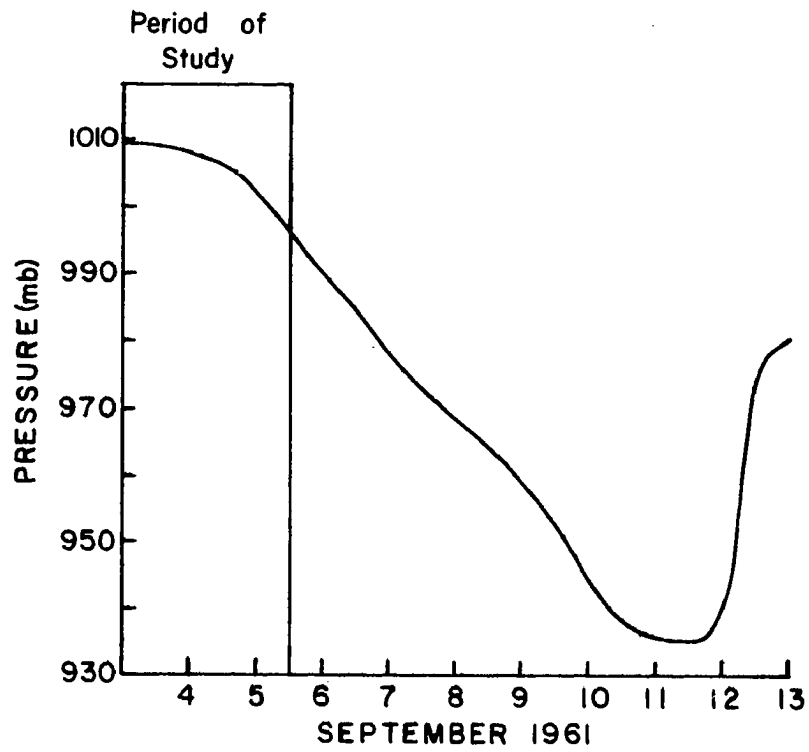
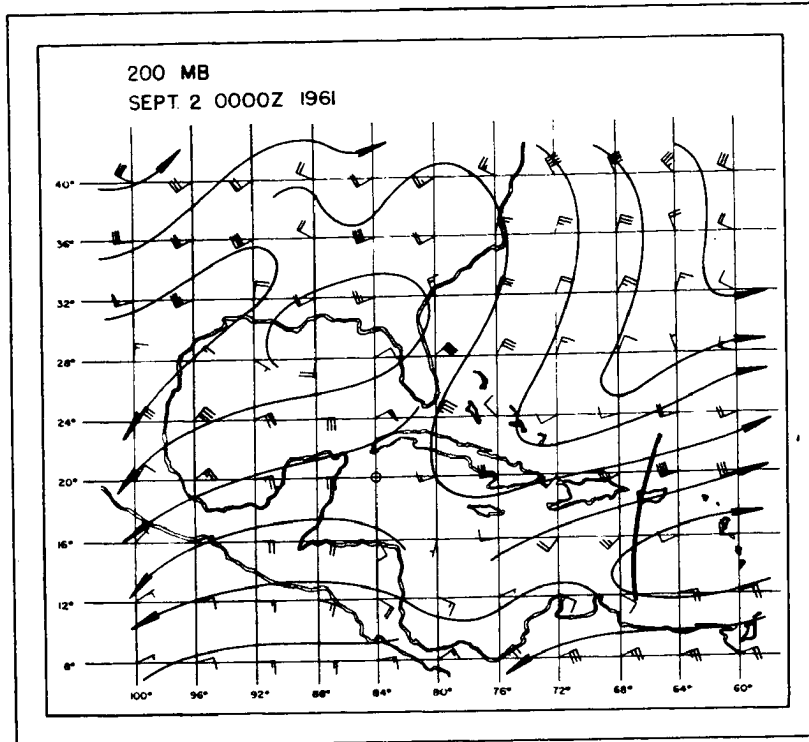


Fig. 6. Central pressure in hurricane Carla for September 4-13, 1961.

A.



B.

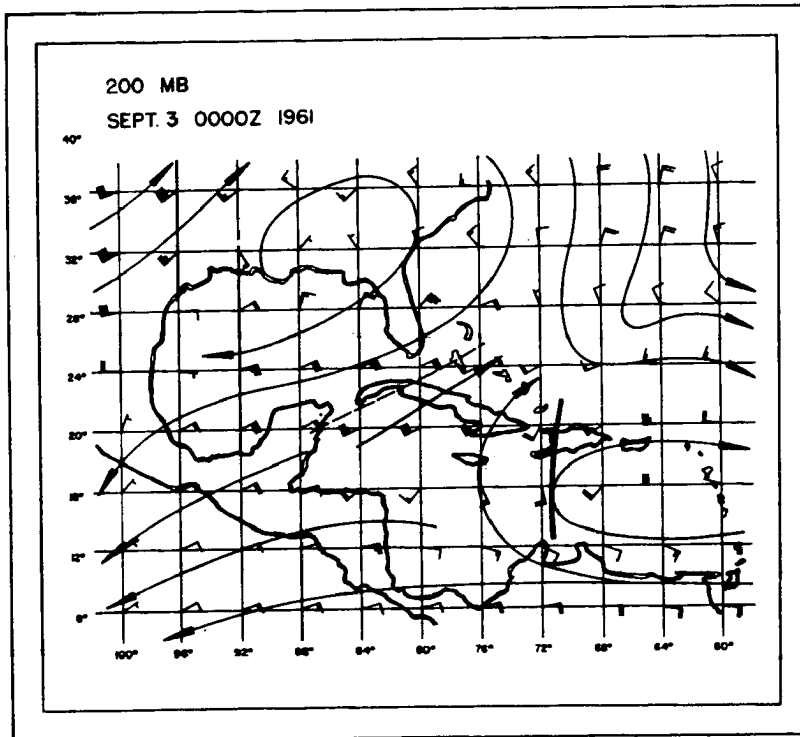
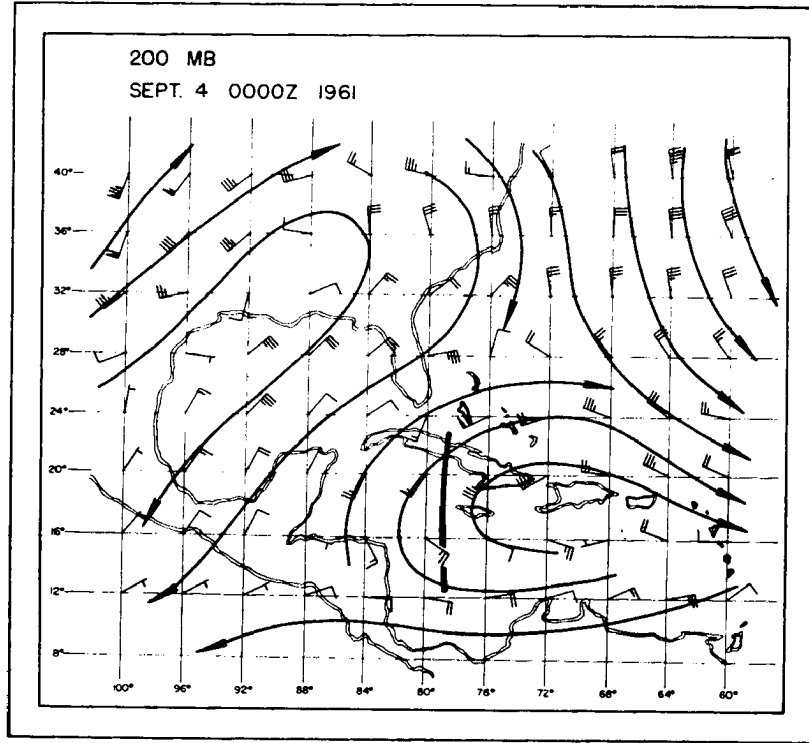


Fig. 7. Wind field at 200 mb at the times indicated for September 2-5, 1961 (development case). Wind speed in knots. The heavy solid lines indicate the disturbance trough at the surface, and the solid dots the position of the vortex at the last two time periods.

C.



D.

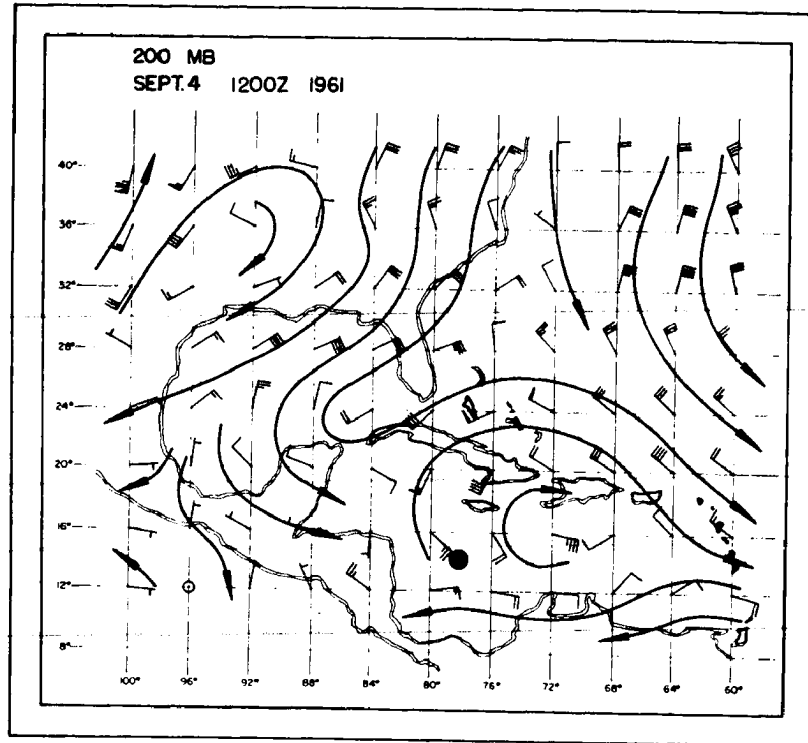


Fig. 7. Continued.

E.

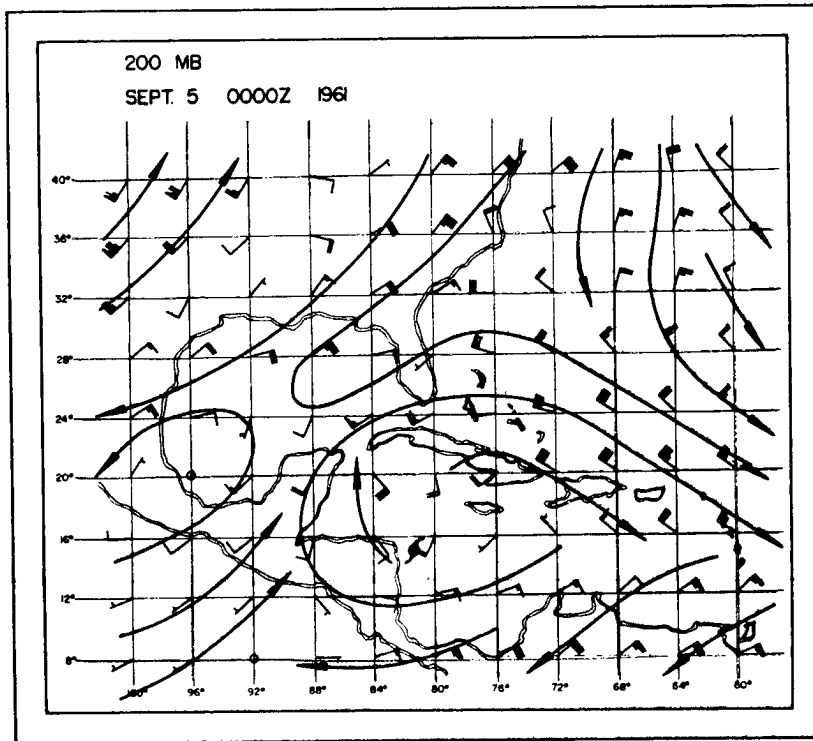


Fig. 7. Continued.

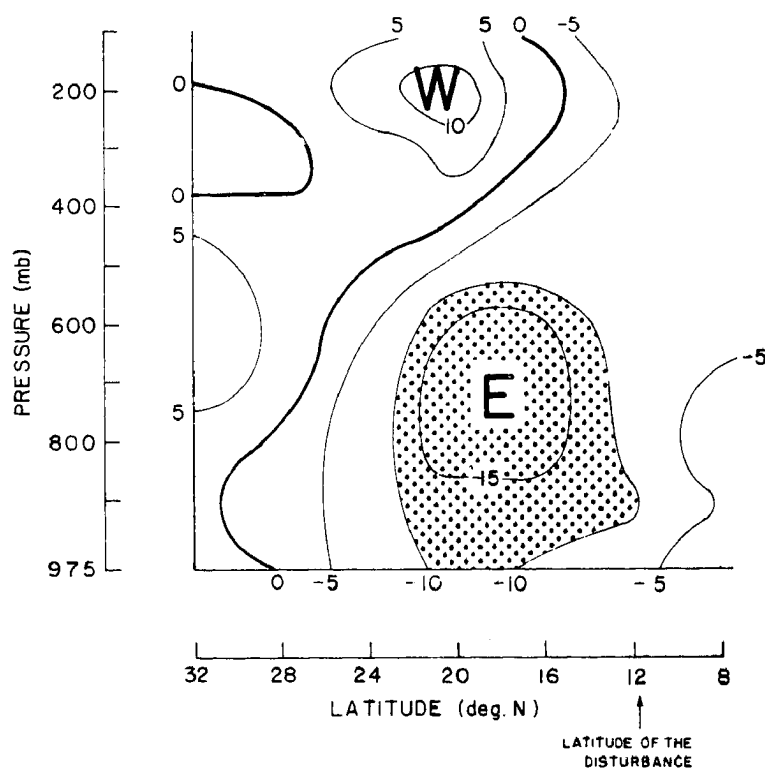
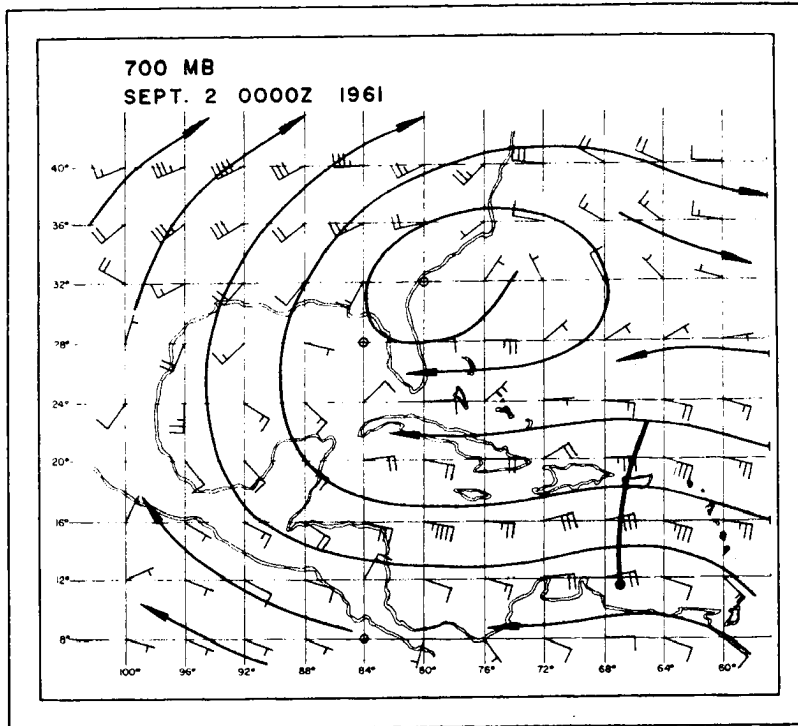


Fig. 8. Zonal wind component (knots). Cross-section along 64° meridian at 1200Z, September 1, 1961 (development case).

A.



B.

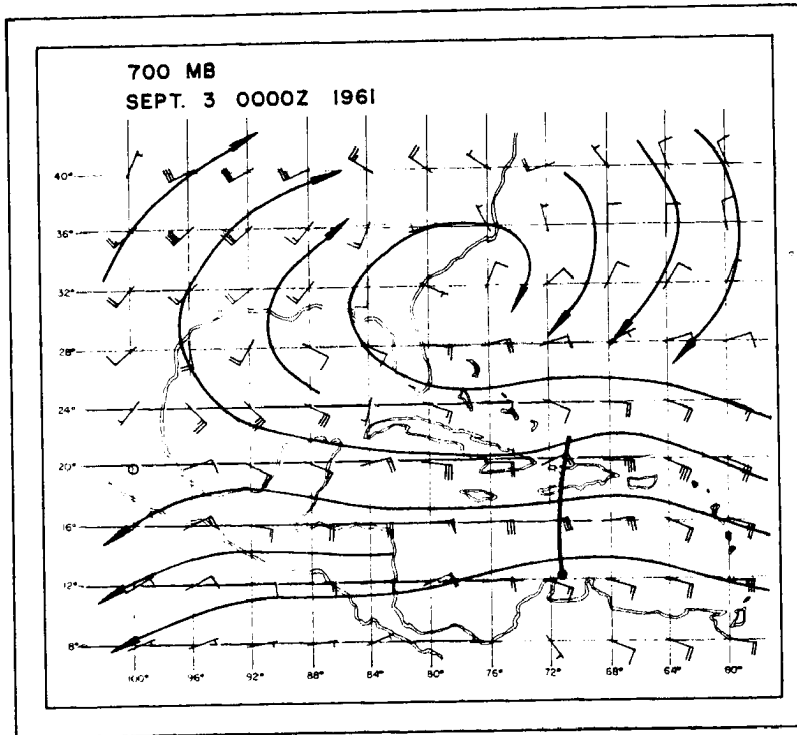
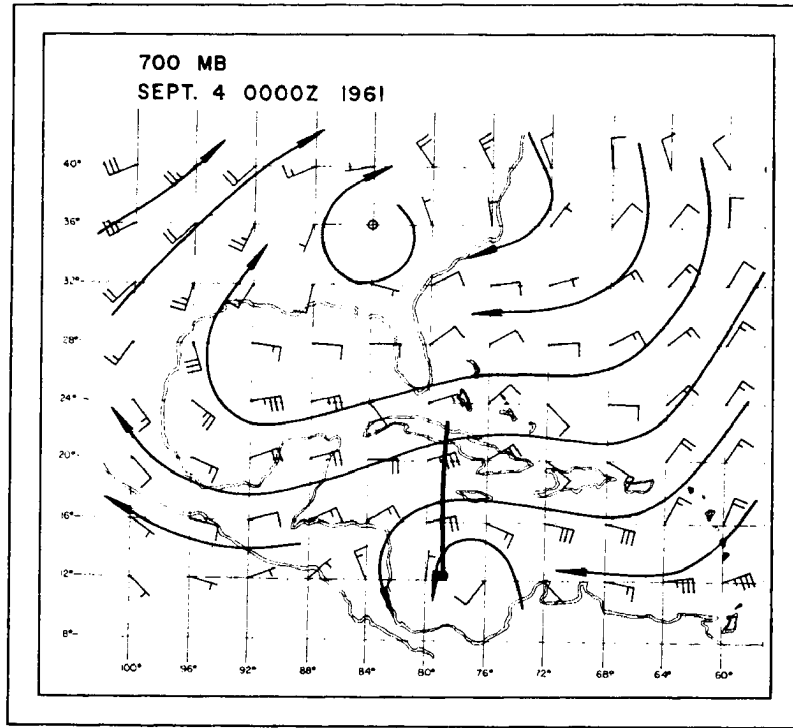


Fig. 9. Wind field at 700 mb at the times indicated for September 2-5, 1961 (development case). Wind speed in knots. The heavy solid lines indicate the disturbance trough at the surface, and the solid dots the position of the vortex at the last two time periods.

C.



D.

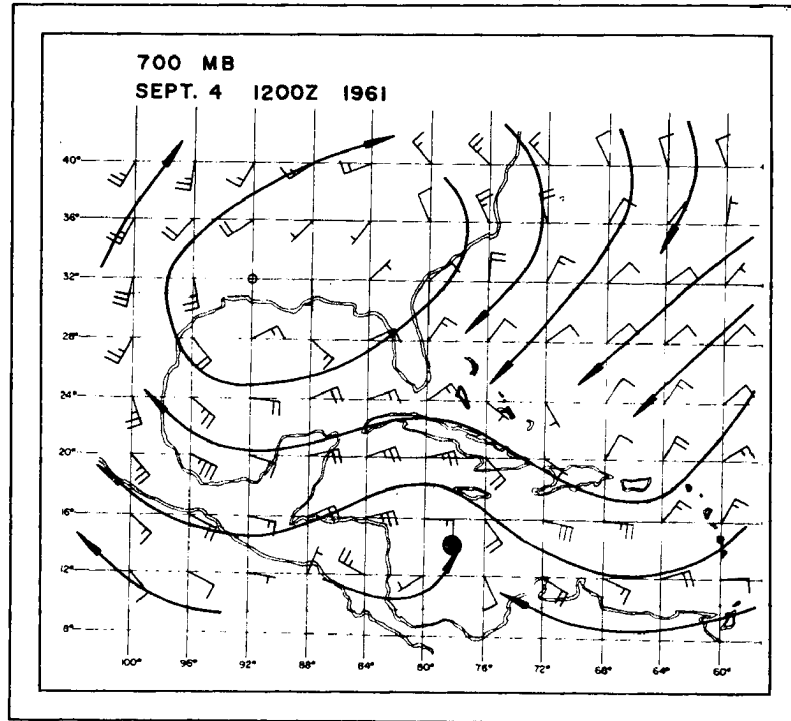


Fig. 9. Continued.

E.

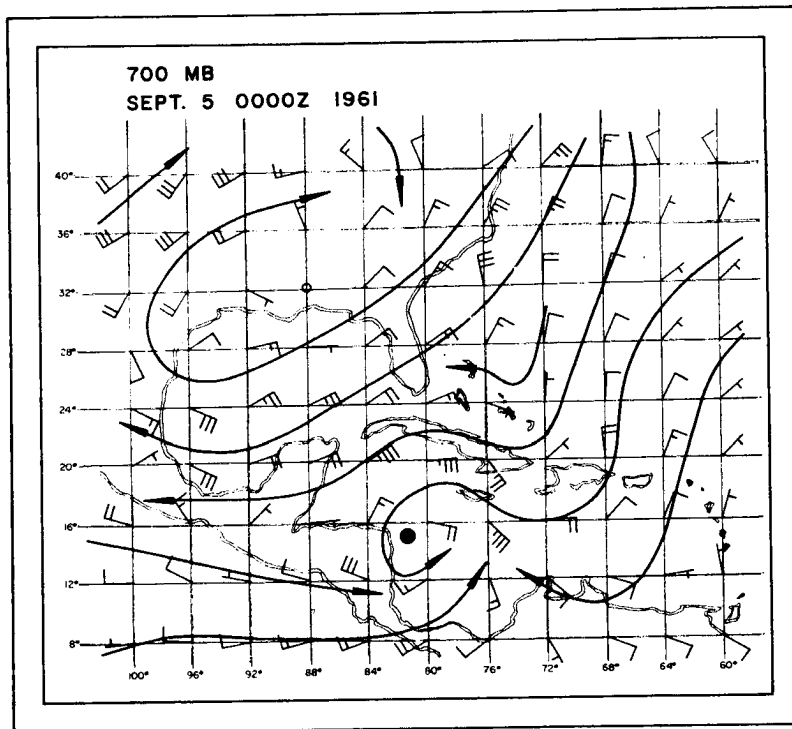
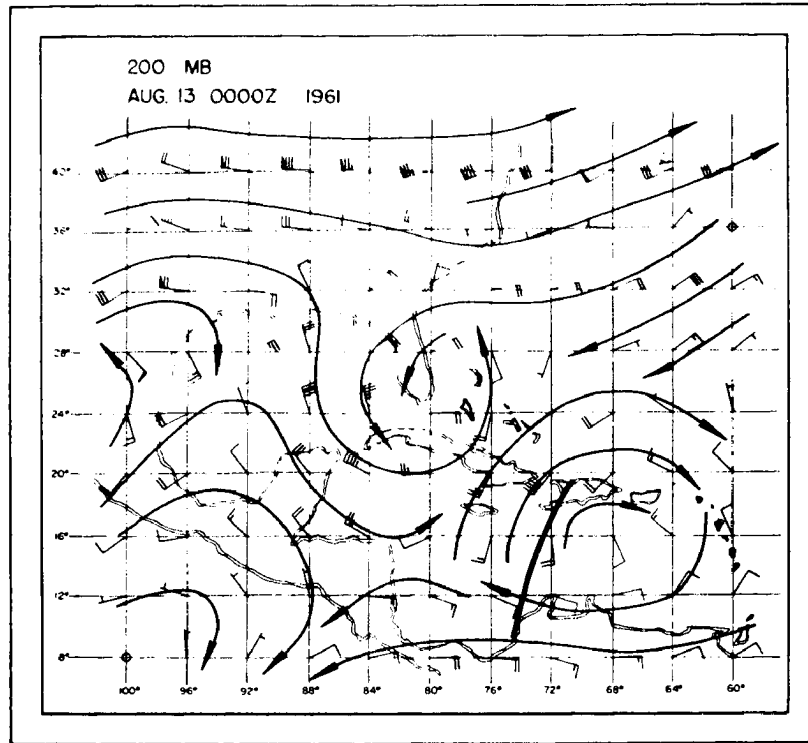


Fig. 9. Continued.

A.



B.

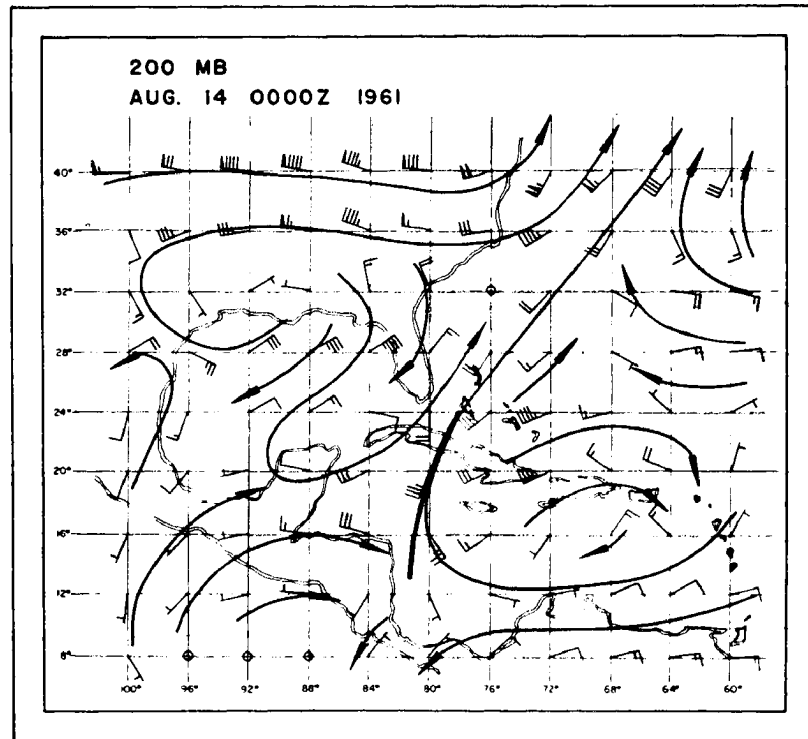


Fig. 10. Wind field at 200 mb at the times indicated for August 13-15, 1961 (non-development case). Wind speed in knots. The heavy solid lines indicate the disturbance trough at the surface.

C.

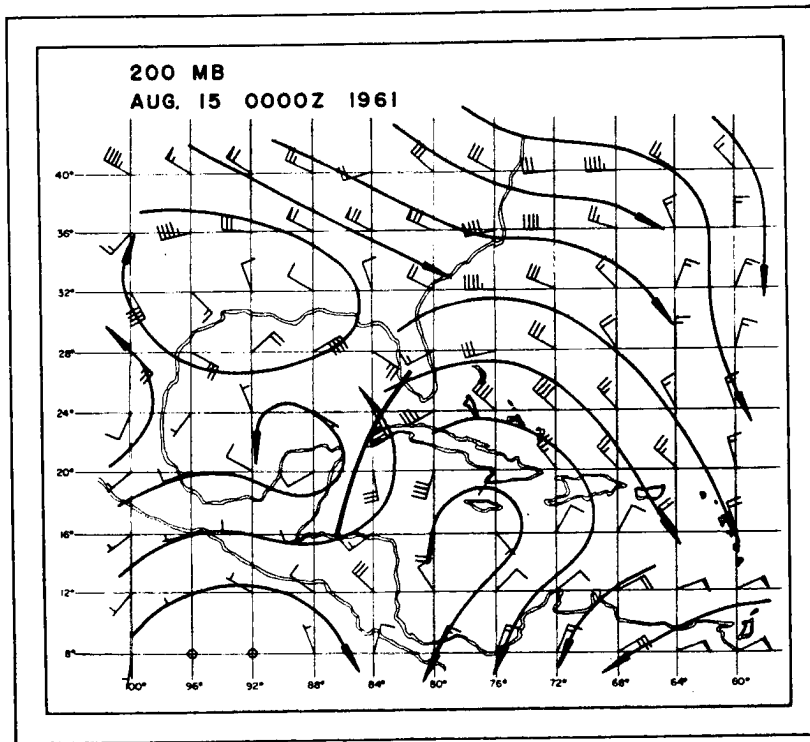
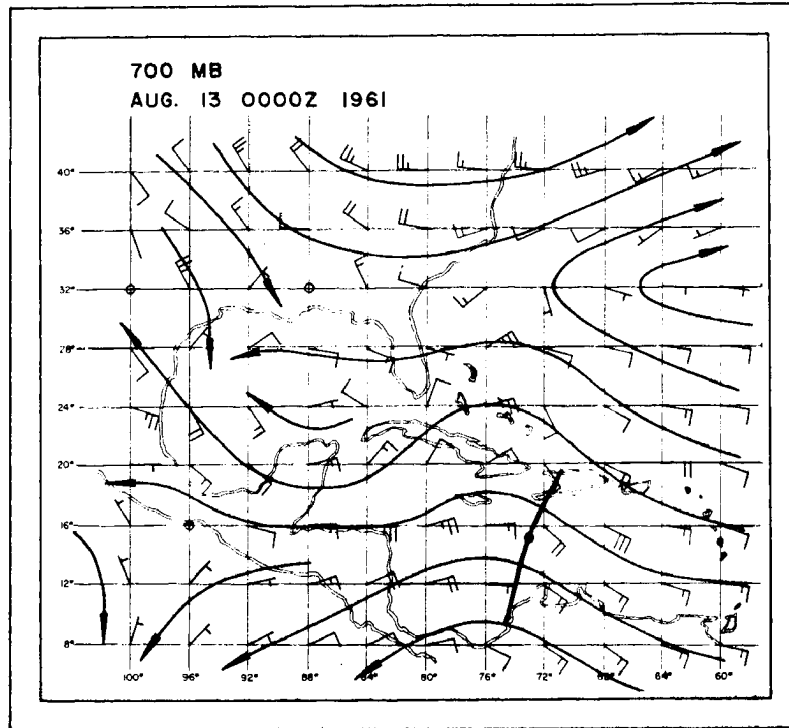


Fig. 10. Continued.

A.



B.

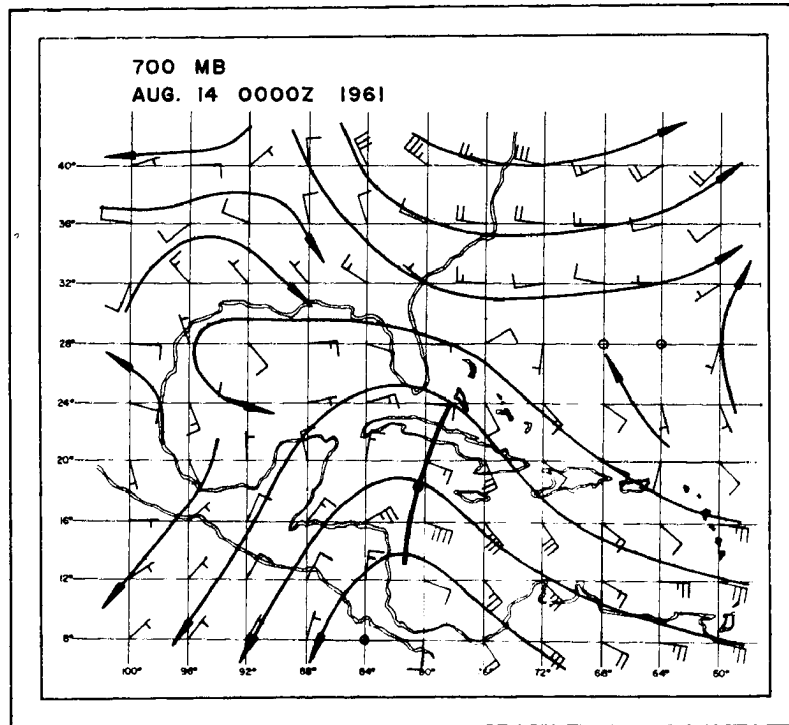


Fig. 11. Wind field at 700 mb at the times indicated for August 13-15, 1961 (non-development case). Wind speed in knots. The heavy solid lines indicate the position of the trough at the surface.

C.

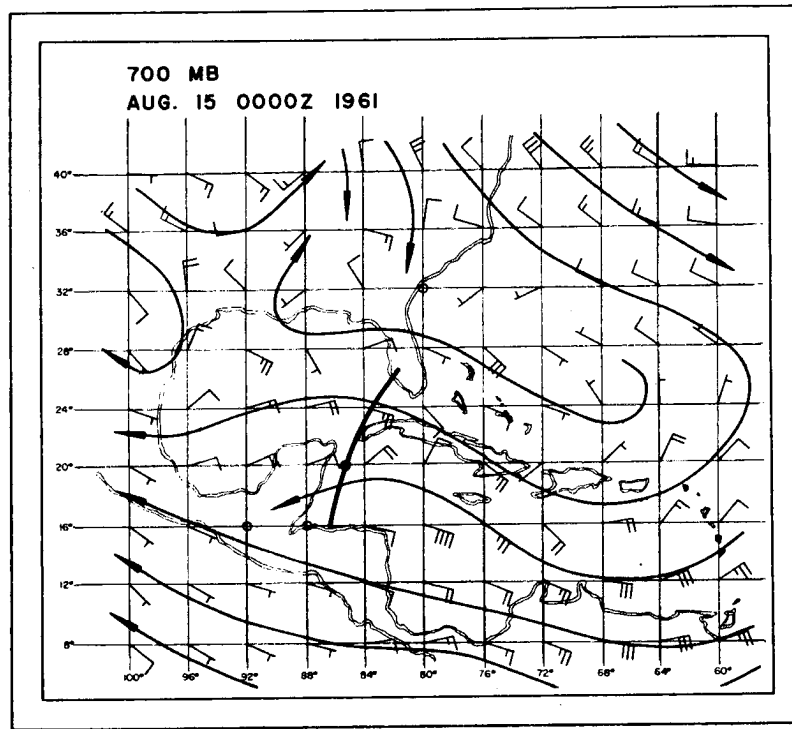


Fig. 11. Continued.

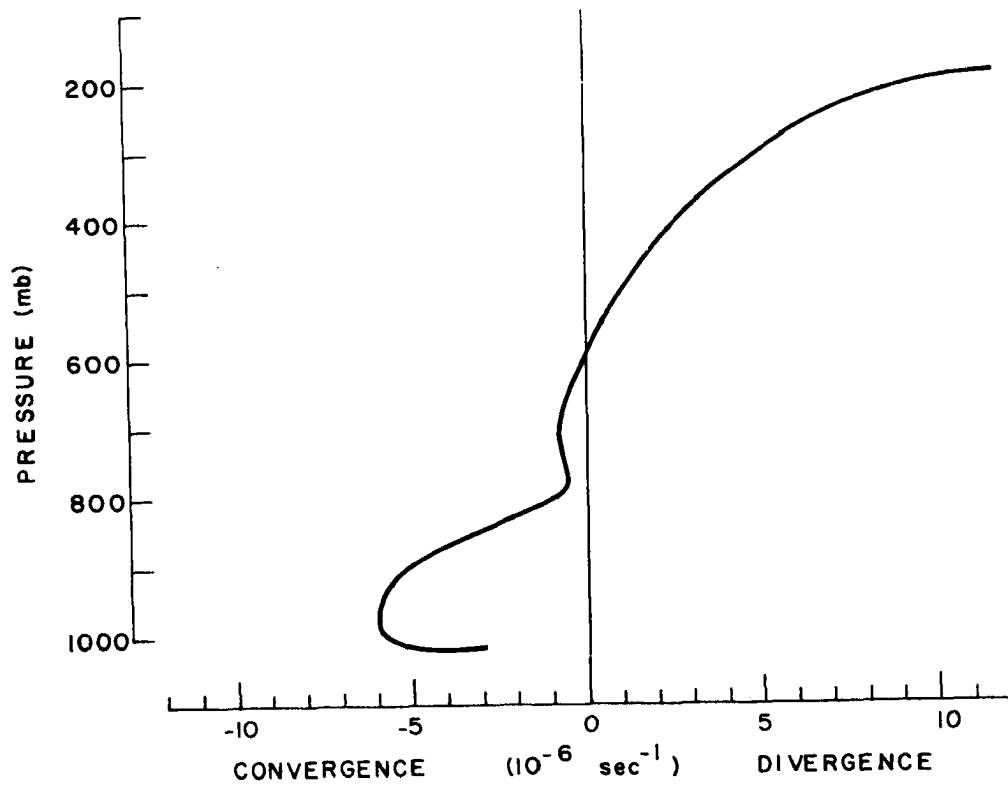


Fig. 12. Average convergence with height in a 3° latitude radius surrounding the center of the developing disturbance during the period of September 3/00Z to 4/12Z. Center was assumed to be at the position of the solid dots of Fig. 9.

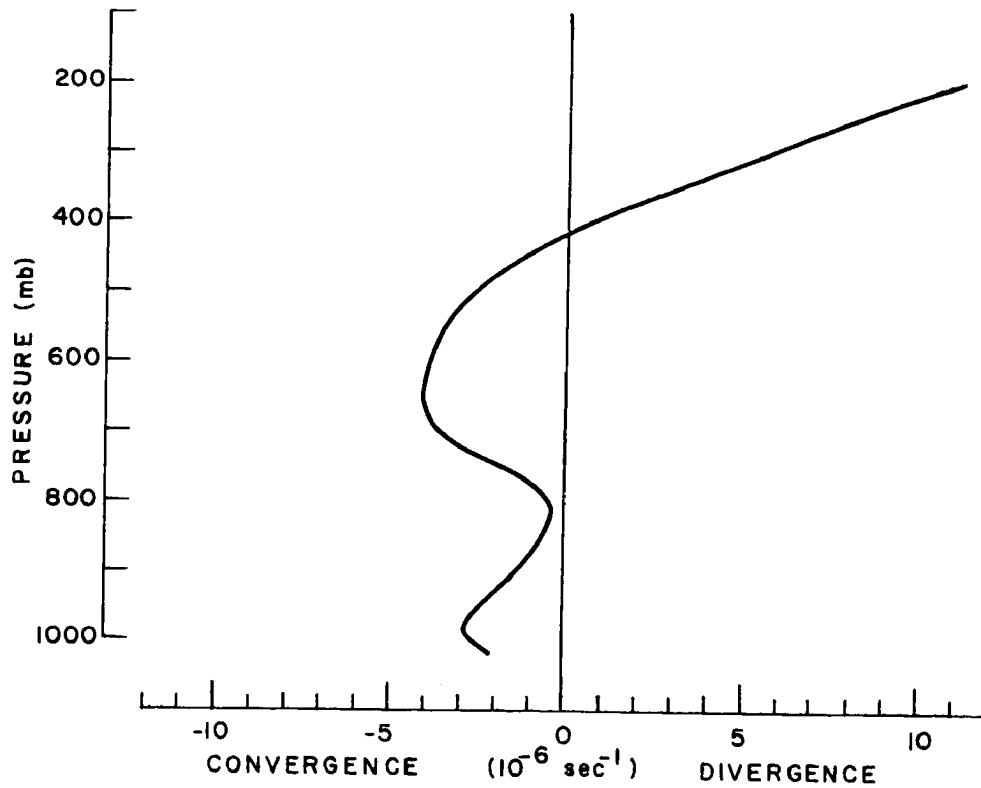


Fig. 13. Average convergence with height in a 3° latitude radius surrounding the center of the non-developing disturbance for the four time periods of 13/00Z to 14/12Z. Center was assumed to be at the position of the solid dots of Fig. 11.

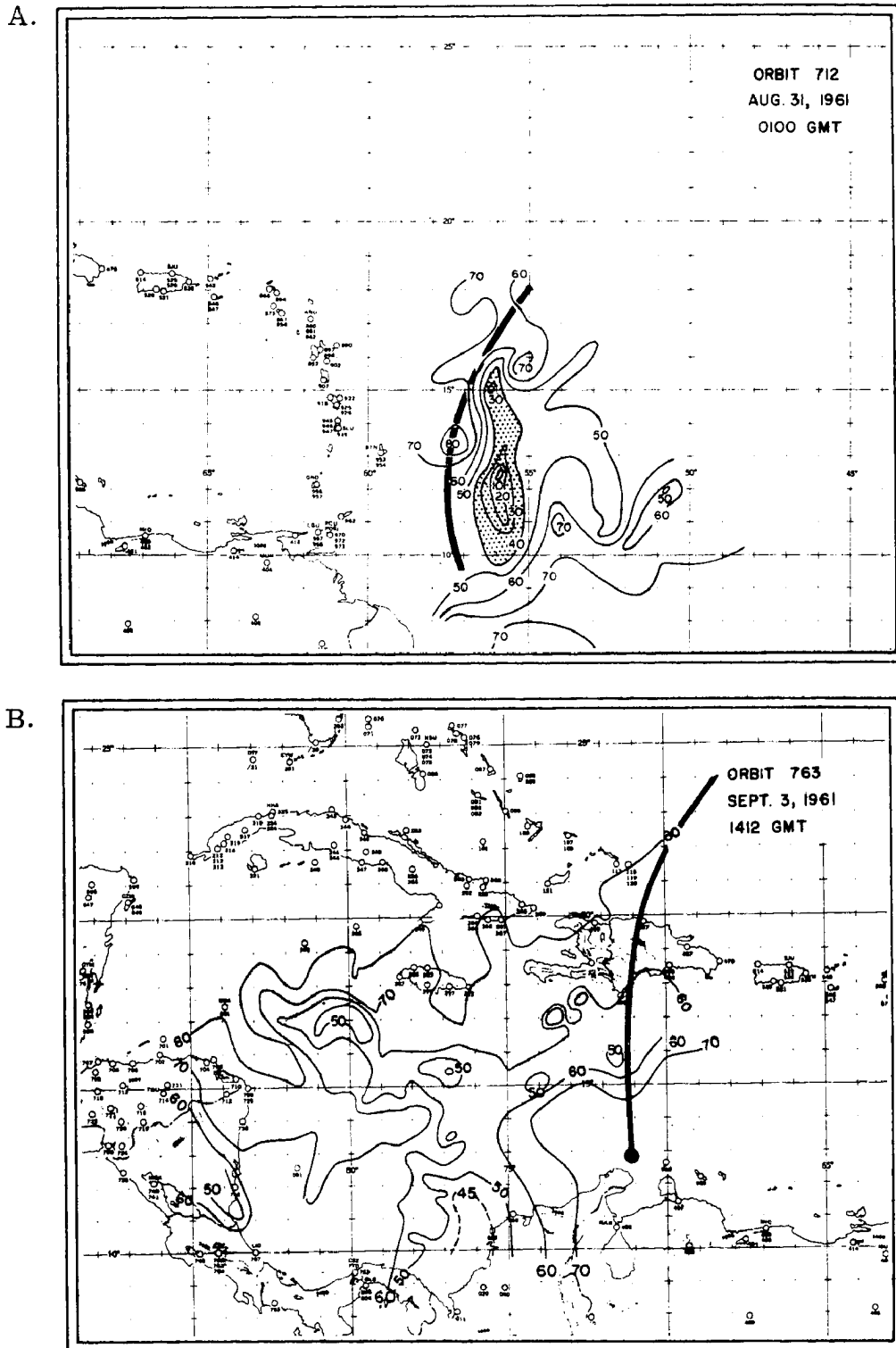


Fig. 14. TIROS III radiation maps, showing equivalent black body temperature (first digit of 2 omitted) in degrees Kelvin at the times indicated for August 31 to September 3, 1961 (development case). Areas colder than 240° K are shaded.

C.

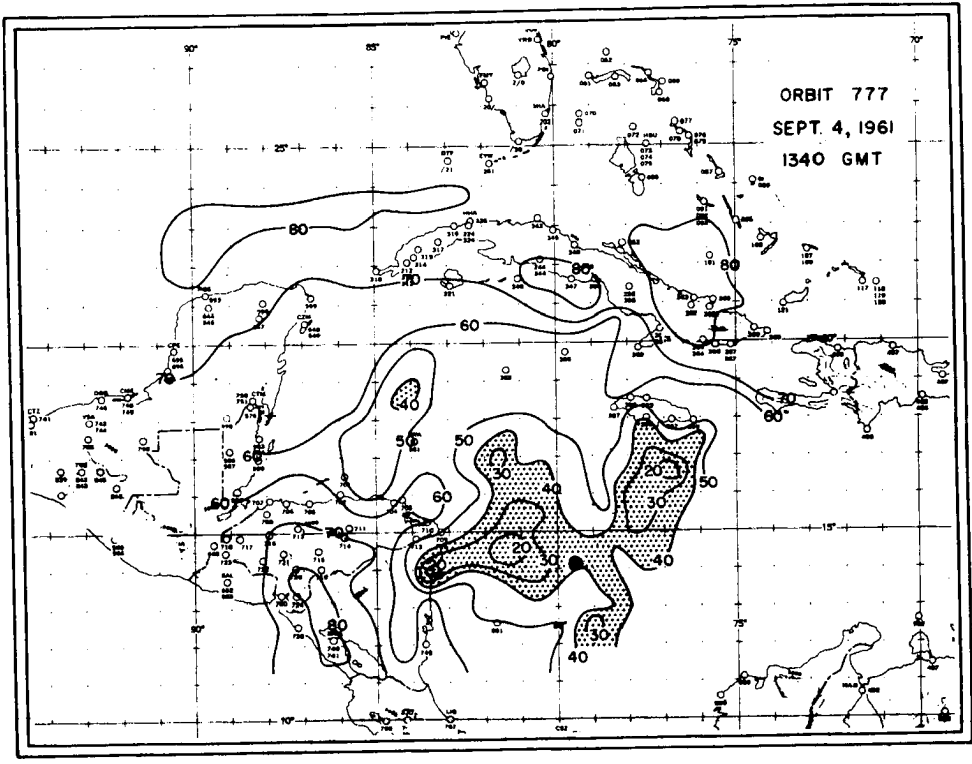
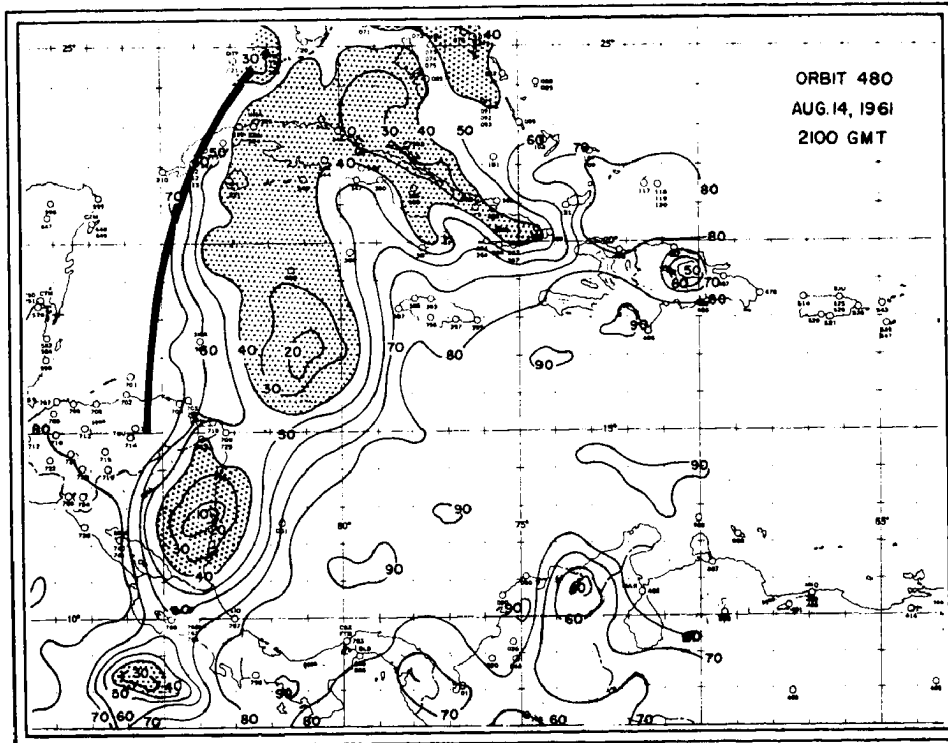


Fig. 14. Continued.

A.



B.

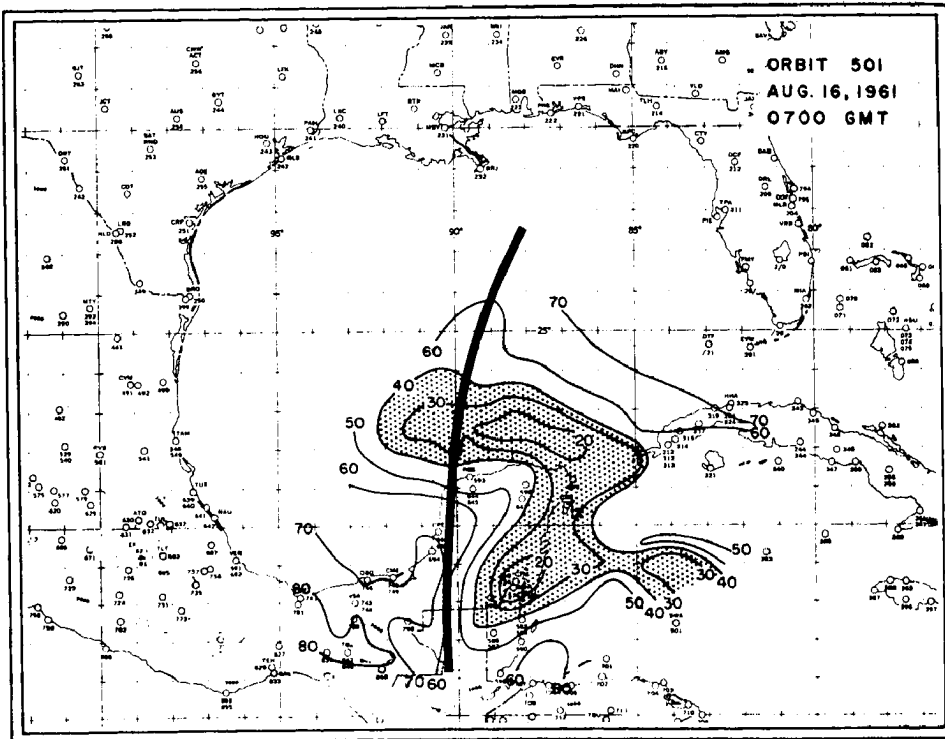


Fig. 15. TIROS III radiation maps, showing equivalent black body temperature (first digit of 2 omitted) in degrees Kelvin at the times indicated for August 14-16, 1961 (non-developing case). Areas colder than 240° K are shaded.

C.

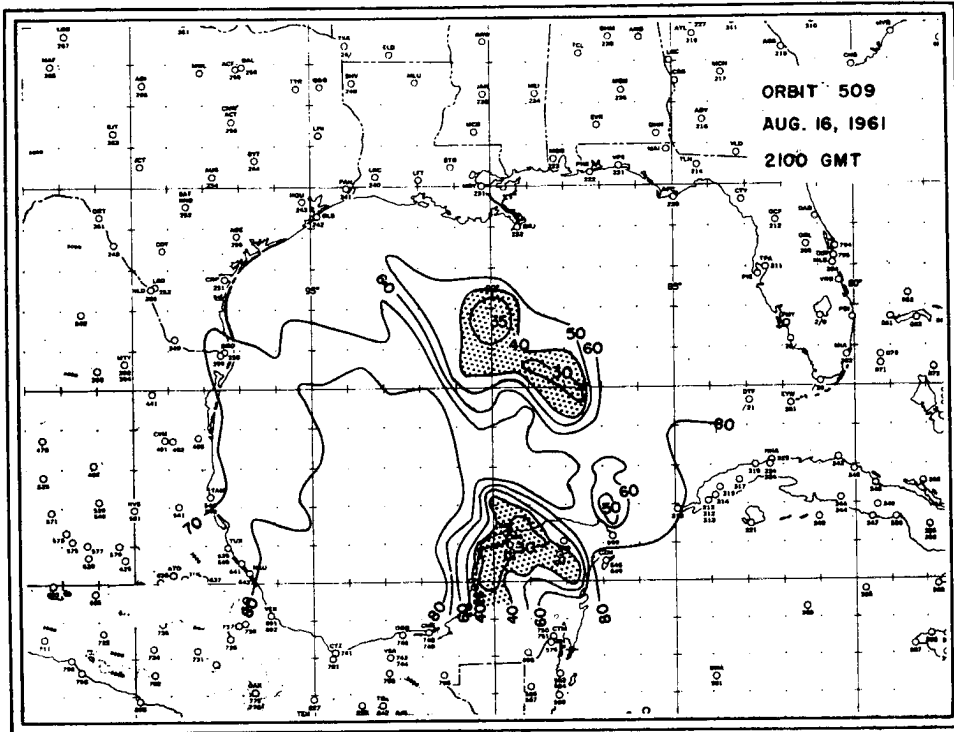


Fig. 15. Continued.

CLOUD RADAR COMPOSITE
4 SEPT., 1961 (1930-0150 GMT)
FLIGHT ALTITUDE 15,600 FT.

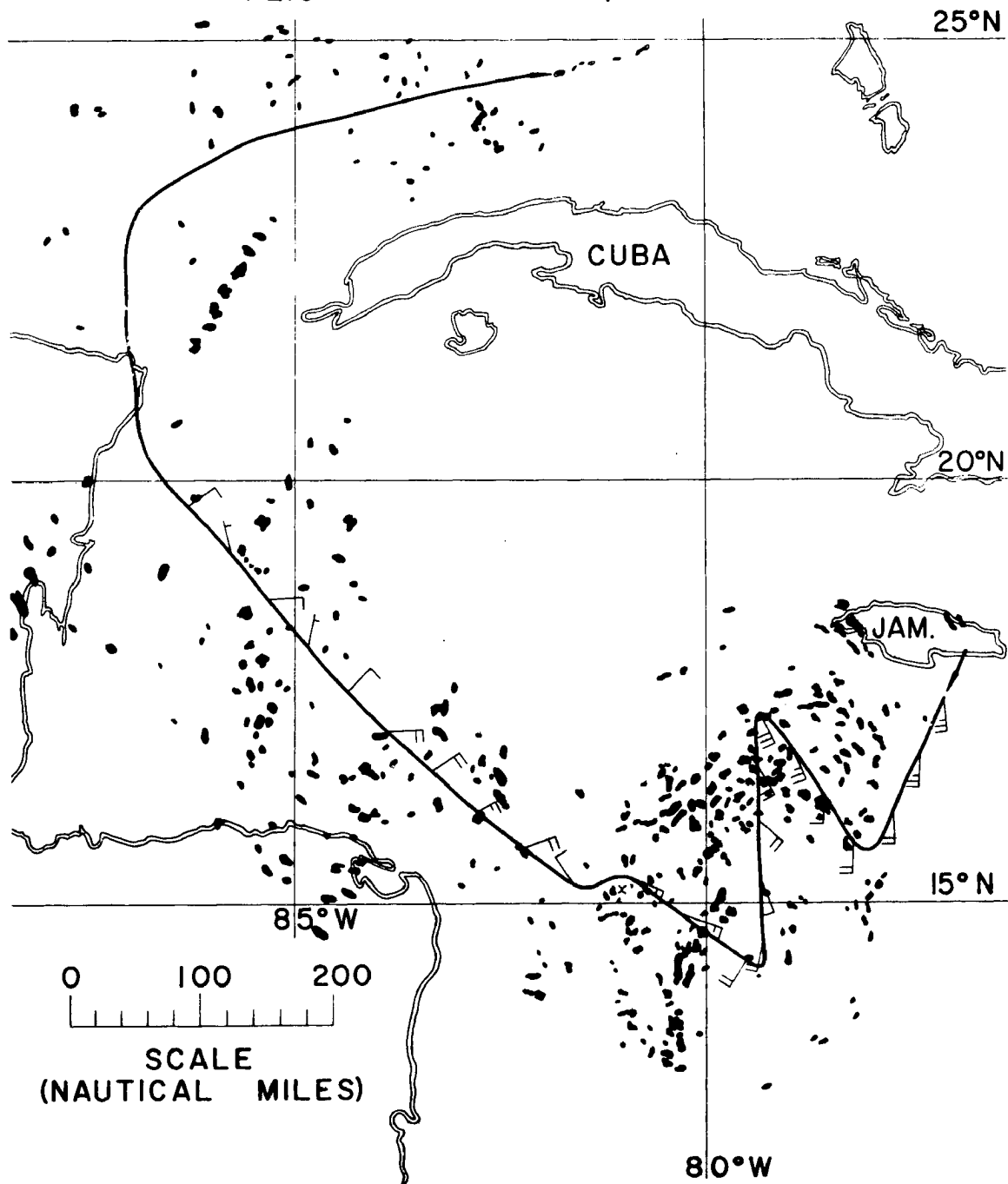


Fig. 16. Radar composite of cumulus rain echoes with 560 mb flight level winds (knots) for September 4, 1961 (development case). Maximum surface winds and minimum sea-level pressure at this time were 50 knots and 1006 mb respectively.

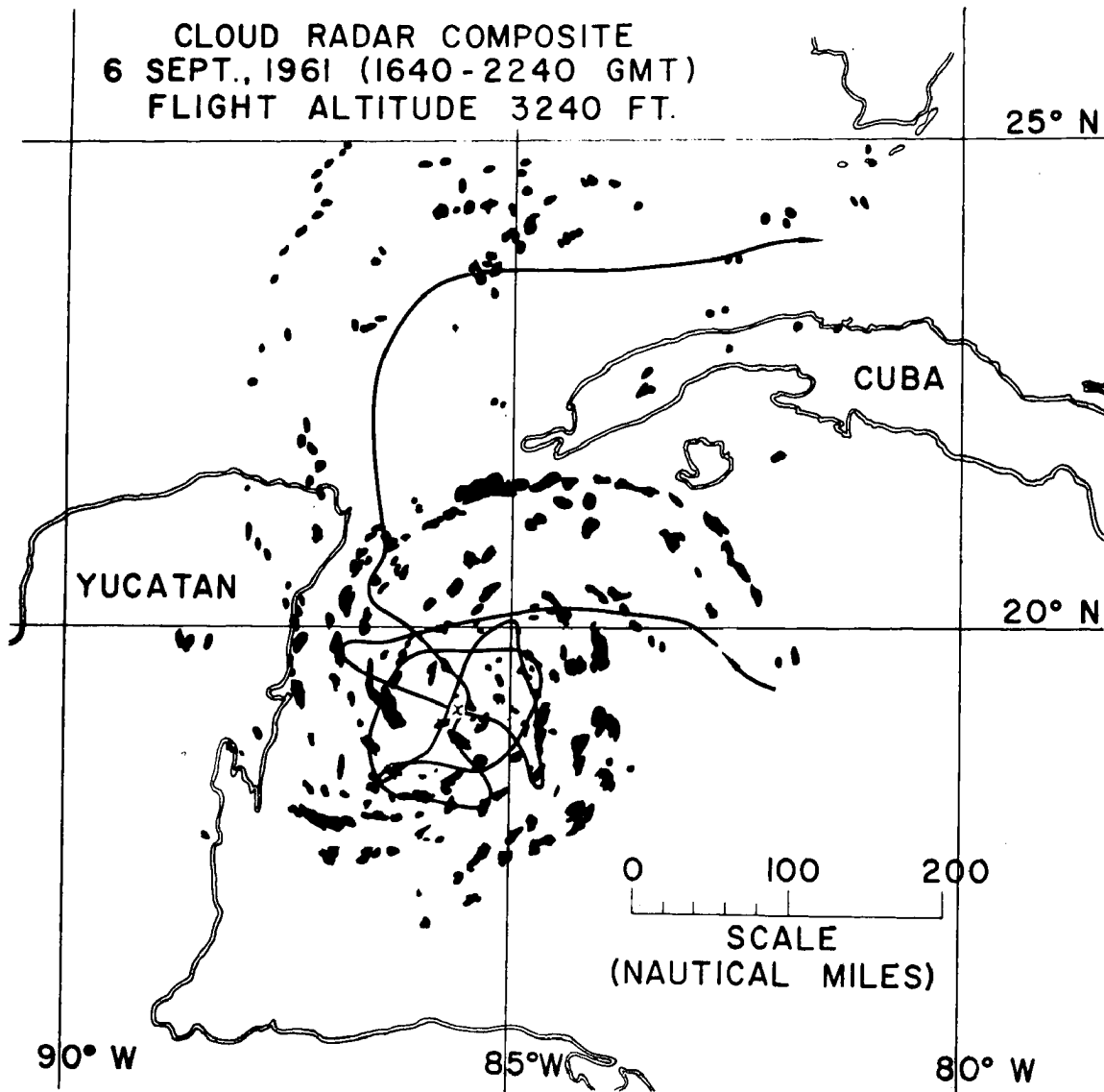


Fig. 17. Radar composite of cumulus rain echoes for September 6, 1961. Maximum surface winds and minimum sea-level pressure at this time were 60 knots and 999 mb respectively. No computations were made at this period of development.

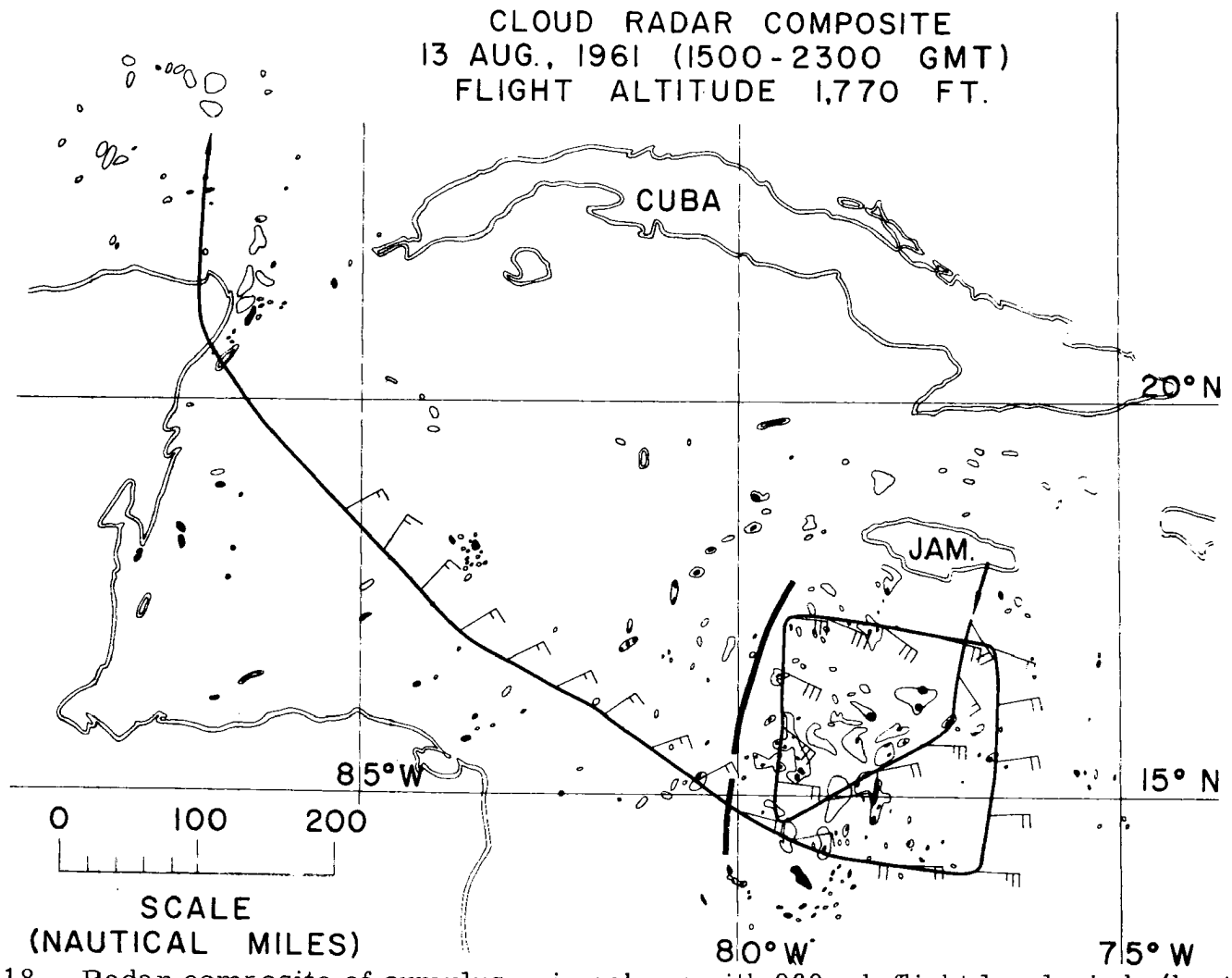


Fig. 18. Radar composite of cumulus rain echoes with 960 mb flight level winds (knots) for August 13, 1961.

CLOUD RADAR COMPOSITE
14 AUG., 1961 (1340-2300 GMT)
FLIGHT ALTITUDE 1,700 FT.

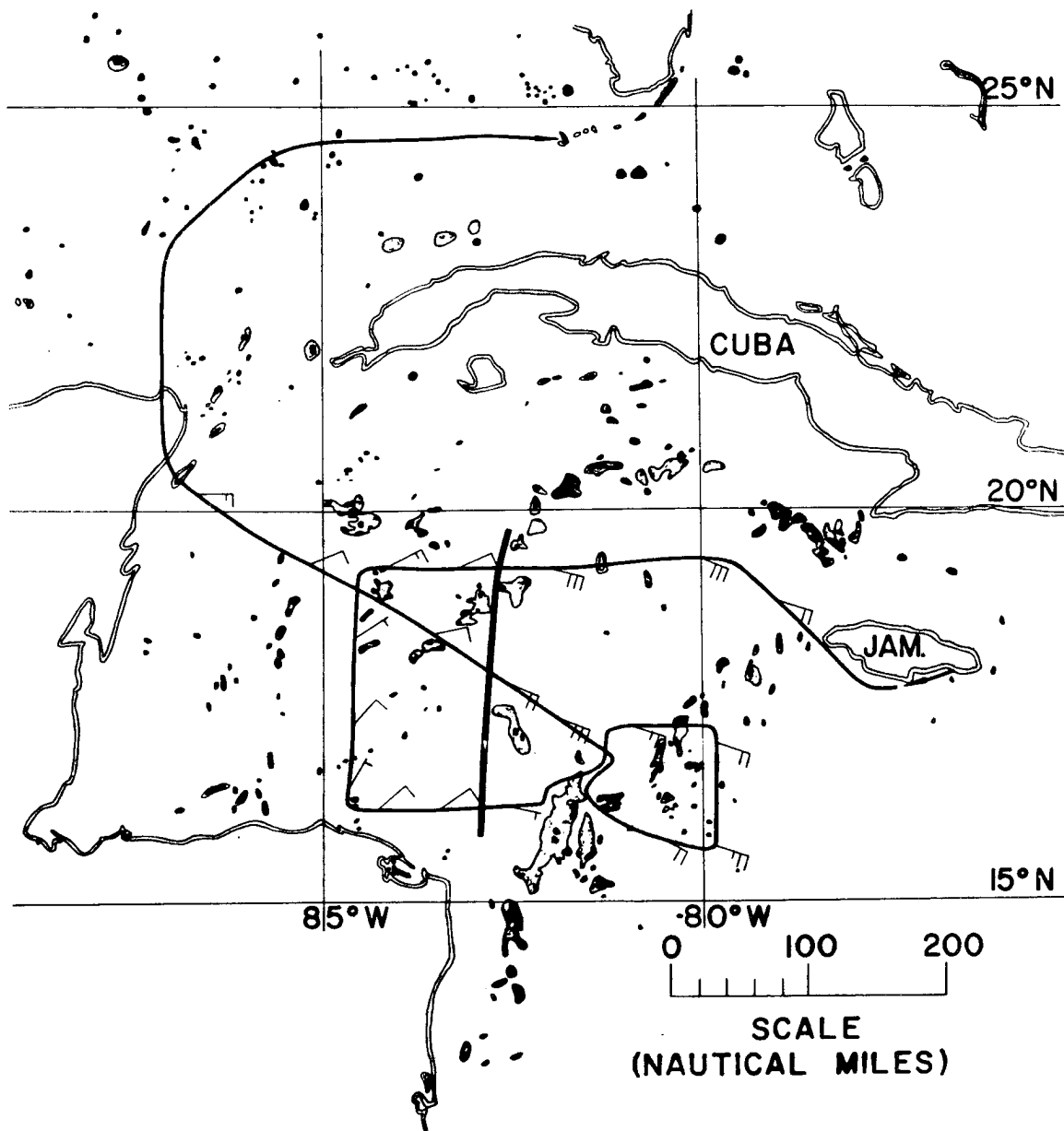


Fig. 19. Radar composite of cumulus rain echoes with 960 mb flight level winds (knots) for August 14, 1961.

IV DEVELOPMENT REQUIREMENTS

One of the basic problems in understanding hurricane development is the lack of knowledge of all of the physical processes which act to produce a drop in surface pressure. The surface pressure of a disturbance decreases (with a lower stratospheric pressure level of no height gradient) when the mean temperature of the troposphere becomes warmer than the environment. Observational studies (Yanai, 1961, 1963; Zipser, 1964) do indeed show that the middle and upper tropospheric temperatures above incipient cyclones are warmer than ambient conditions. Release of latent heat of condensation in cumulus clouds has been generally accepted as the reason for these temperature rises. This heat source is in turn dependent on the magnitude of the convergence in the layer beneath the bases of cumulus clouds, which over the tropical oceans are observed to be approximately at 950 mb (600 meters).

Charney and Eliassen (1949, 1964) have discussed the importance of frictional or Ekman turning of the wind as an important producer of surface convergence and vertical motions at the top of the surface boundary layer. Gray (1967b) has presented observational evidence of a significant frictionally induced boundary layer wind veering over the tropical oceans. This frictional veering produces sub-cloud layer convergence in regions of cyclonic horizontal wind shear. This is envisaged as crucial in establishing the initial water vapor convergence required for disturbance genesis.

Convergence above the base of the cumulus clouds, on the other hand, plays an entirely different role. Fig. 20 shows that only air which rises from levels below 900 mb can warm the surrounding environment. With the lapse rates and relative humidities of the tropical environment, vertical motions arising from convergence above 900 mb produce a net cooling of the troposphere. Initial dry adiabatic expansion of the air parcel thus produces a reduction of temperature that is larger than the subsequent condensation warming.

Where active cumulus convection has been occurring, moisture is raised to higher levels. Fig. 21 is representative of a sounding for average moisture conditions in the two disturbances considered in this study. This sounding is nearly identical to all disturbance soundings from which tropical storms develop. Although the level of effective warming from condensation has been raised somewhat, it is still apparent that the cooling due to ascent from middle level convergence can be compensated for only if a larger net convergence occurs below 850 mb.

A large warming due to water vapor convergence does not by itself imply that the troposphere above a surface disturbance will warm sufficiently to produce a vortex. A vortex will develop only under conditions favorable for the accumulation and concentration of the latent heat over a small area. If existing flow conditions cause an evacuation of the condensed heat away from the disturbance

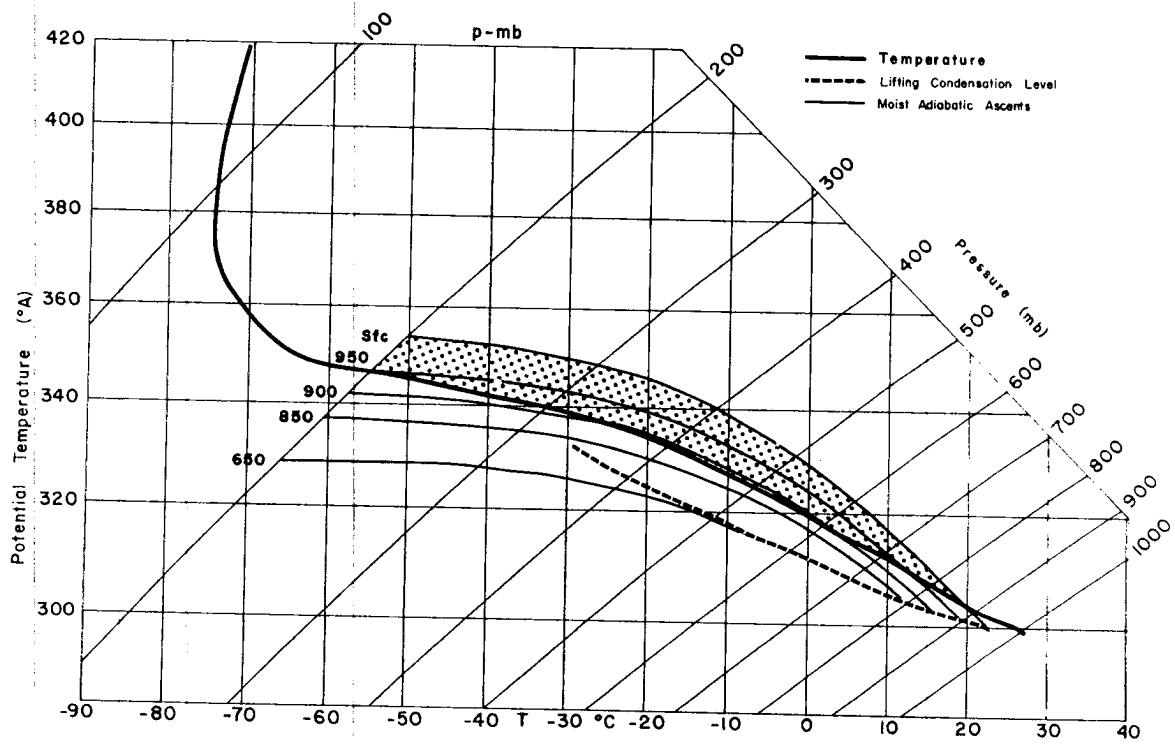


Fig. 20. Mean sounding for Swan Island for the month of August, solid line, after Jordan (1957). Numbers in the left center portion of figure represent parcel ascent beginning at the pressure levels indicated. Shaded areas represent positive temperature anomalies of raising undiluted parcels.

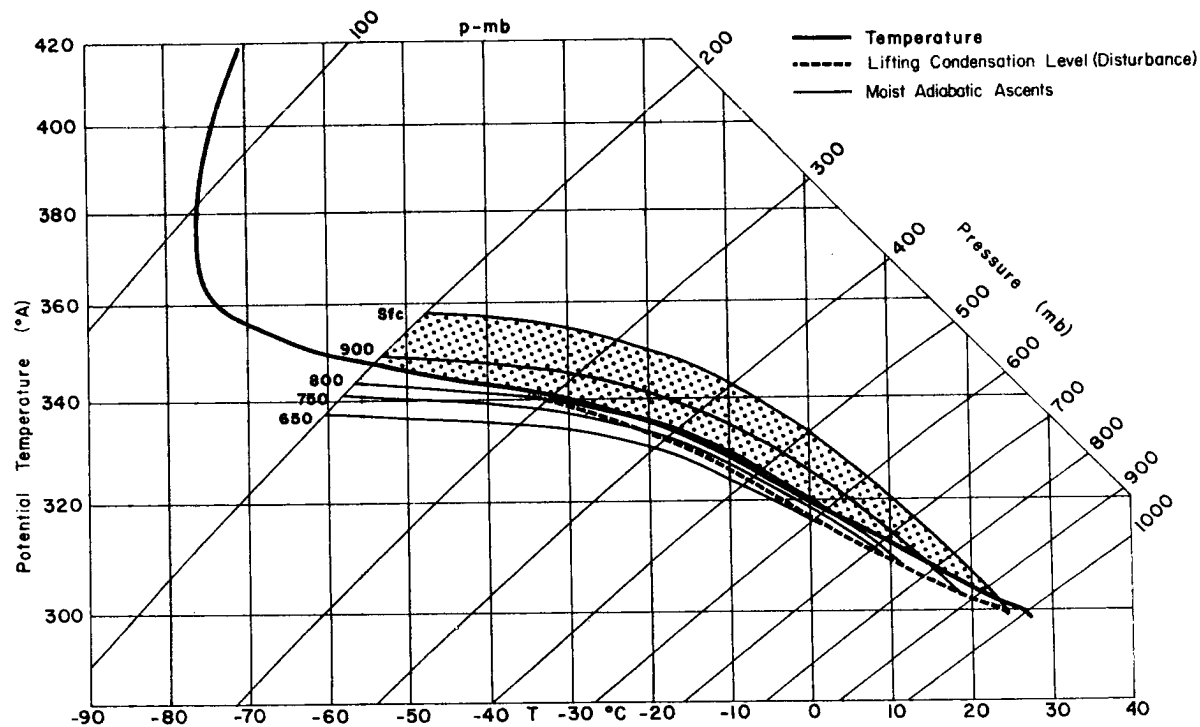


Fig. 21. Mean sounding for the cloud areas of the two disturbances. This sounding is typical of the summertime tropical disturbance areas. Numbers in the left center portion of figure represent parcel ascent beginning at the pressure levels indicated. Shaded areas represent positive temperature anomalies of raising parcels. Condensation levels typical of a disturbance in the easterlies.

or produce too much mixing with the cooler exterior environmental air, development will be very slow or will not result. In fact, most of the intense tropical rain areas do not produce tropical storms because of these restraining mechanisms. The importance of tropospheric heat accumulation has been a neglected topic of development discussions. It is usually taken for granted that the latent heat remains over the system.

There are two primary factors which inhibit tropospheric accumulation of heat. These are:

- 1) Strong flow of the environmental air relative to the disturbance motion. This brings cooler surrounding ambient air through the disturbance and an accumulation of heat is inhibited. This "ventilation effect" might be approximated by the tropospheric vertical wind shear.
- 2) Upper level divergent outflow which will carry away part of the enthalpy gained from the released latent heat. The mean divergence aloft is, however, crucially necessary for development.

If the combined interaction of heat sources and sinks results in a continuous net warming of the troposphere, vortex development becomes possible. Tropical disturbance intensification is envisaged as follows:

As the troposphere warms with an upper pressure level of no height gradient, expansion is produced and mass

is evacuated from the system. The reduction of the mass in a tropospheric column requires, hydrostatically, a reduction in the pressure at the surface. The winds respond to the increasing pressure gradient and are accelerated, thus increasing the low-level frictional convergence. The cumulus convection is in turn enhanced. The resultant warming in the upper troposphere induces further expansion and outflow of mass from the disturbance. Due to the expansion produced from latent heat release, the upper outflow is greater than the low-level inflow, and the surface pressure is thus further reduced. As the process continues, the temperature contrasts between the storm and the environment increase. The characteristics of the tropical vortex then follow.

Figs. 12 and 13 of the last section showed that the developing disturbance had a larger sub-cloud convergence than the non-developing case. As the potential condensation warming depends directly on the low-level moisture inflow, the developing case is observed to have a twofold advantage in condensation heating potential over the non-development case. In addition, the very large middle level convergence and larger vertical wind shear of the non-developing disturbance greatly reduced this already smaller heating potential. The disturbance that developed into hurricane Carla had, qualitatively, in its earlier stages, an intensification

potential four or five times larger than the non-developing case.

This intensification potential was not at all obvious in the synoptic charts or cross-sections. A quantitative assessment of these warming factors is presented in the next section.

V QUANTITATIVE ASSESSMENT OF DISTURBANCE HEATING PROCESSES

Having discussed the heating factors that control disturbance development, we will now attempt to obtain an estimate of their magnitudes. In addition, we will try to develop a simple physical model that describes the interrelation of these factors in time. In order to keep the basic concepts of the model as clear as possible, the thermodynamics of the heating process will be isolated and considered by itself. The detailed flow dynamics will be considered only in regard to its influence on the processes that lead to production and accumulation of heat in the disturbance. The dynamic and kinematic fields will be derived from the objective analyses of the synoptic data.

This study concerns itself only with the early stages of disturbance development i. e. , the period between the time a well defined disturbance is observed up to the time a well established vortex circulation is present. The later stages of hurricane intensification have been the subject of many studies and detailed numerical models and will not be considered in this investigation. For this reason, only the four 12 hour periods from 00Z, 3 September through 12Z, 4 September will be considered for the developing disturbance. An equal number of four 12 hour time intervals are treated (00Z, 13 August through 12Z, 14 August) for the non-developing case as it traveled through the same region two weeks earlier.

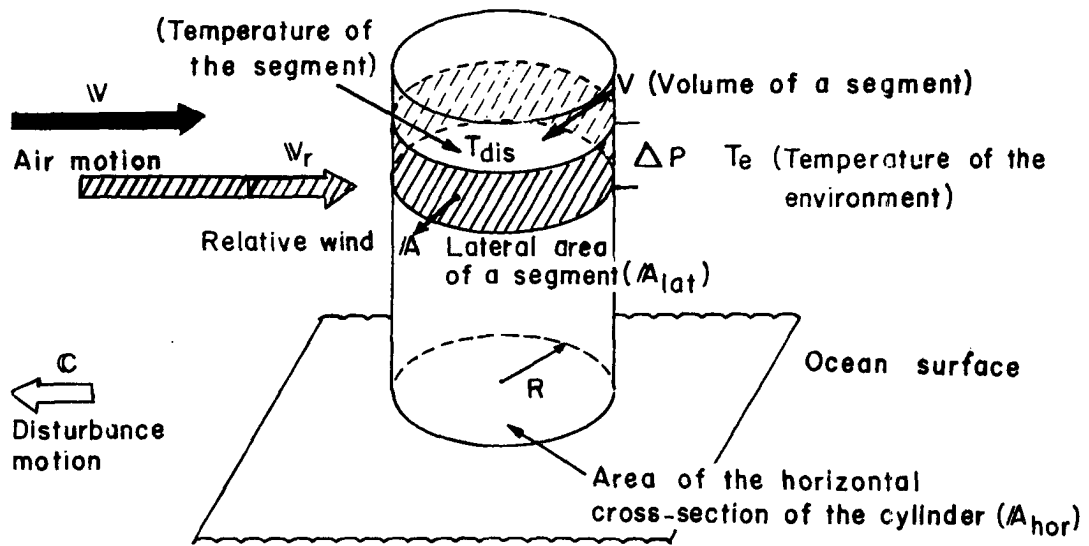


Fig. 22. Diagram depicting the geometrical scheme used in performing the various computations. This cylinder of radius R (3° Latitude) extends from the surface to 150 mb, encloses the disturbance, and is divided into elemental cylindrical sections of 100 mb pressure depth (Δp). These elemental segments have a volume V and a lateral vertical area A_{lat} . The horizontal cross sectional area of the cylinder is denoted as A_{hor} . The average temperature of any segment inside the disturbance is T_{dis} , while outside, in a layer at the same pressure level the temperature is designated by the symbol T_e .

Heat budget computations were performed in steps of 12 hours for both cases. The geometrical scheme utilized was as follows: Consider each of the disturbances enclosed in a cylinder of 3° latitude radius (R) and extending from the surface to 150 mb and whose axis was located over the surface center of the disturbance. The area of this cylinder includes most of the convective activity. Furthermore, let us divide this volume into shallow horizontal cylinders of 100 mb pressure thickness Δp (see Fig. 22). These volume segments are referred to as "elemental cylindrical sections". Computations of the average heating and cooling will be performed for each of these segments.

The symbols used in these calculations are indicated in Table 1.

Heat Sources

Sub-cloud layer convergence. In most of the recent models of hurricane development (Ooyama, 1963; Charney and Eliassen, 1964; Ogura, 1964; Kuo, 1965; Syono and Yamasaki, 1967) the effect of the cumulus clouds on the broad scale system has been parameterized in terms of the low-level convergence or the resultant vertical velocity at the top of the boundary layer. The water vapor brought in by the low-level convergence is assumed to ascend and condense within cumulus clouds. This latent heat of condensation is principally released in cumulonimbus "hot towers" which eventually decay and mix with the environment.

TABLE 1

Symbols for Constants and Variables

Basic

t: Time

Δt : Interval of time

p: Pressure

T: Temperature

q: Specific humidity

q_0 : Specific humidity of the surface air

ρ : Density of air at a given pressure level

L: Latent heat of condensation

c_p : Specific heat of air

—: (Bar) over a quantity represents a twelve hour average

M_i : Mass in the inflow region in the sub-cloud layer

Geometrical (See Fig. 22)

A_{hor} : Area of the horizontal cross section of the 3° latitude radius cylinder enclosing the disturbance

A_{lat} : Lateral vertical area of the elemental cylindrical section

V: Volume of an elemental cylindrical section $(\pi R^2 \Delta z)$

m: Mass of an elemental cylindrical section $(\pi R^2 \frac{\Delta p}{g})$

Δp : Pressure depth of an elemental cylindrical section

Kinematic

\mathbf{v} : Vector velocity of the wind at any level

\mathbf{v}_r : Vector velocity of the wind relative to the disturbance ($\mathbf{v} - \mathbf{C}$),
where \mathbf{C} is the vector velocity of the disturbance and \mathbf{v} is the
velocity of the wind at any level

$\nabla_2 \cdot \mathbf{v}$: Horizontal wind divergence

\mathbf{C} : Vector velocity of the disturbance

Thermodynamic

T: Temperature of the air

T_{dry} : Temperature at any pressure level resulting from dry
adiabatic expansion from cumulus cloud base at 950 mb

T_{moist} : Temperature at any pressure level resulting from
moist adiabatic expansion from cumulus cloud base
at 950 mb

T_e : Temperature at any pressure level of the environment
air outside the disturbance

T_{dis} : Average temperature of the disturbance inside an
elemental cylindrical section

T_{ce} : Temperature at any pressure level of the air
surrounding cumulus clouds

ΔT_{dis} : Change of the temperature of the disturbance inside an
elemental cylindrical section resulting from the cumulative
effect of the heat sources and sinks during the 48 hour period
of consideration

ΔT_a : Temperature difference in ° C between the hurricane season
tropical atmosphere and the equivalent dry adiabatic tempera-
ture for ascent from 950 mb ($T_{ce} - T_{dry}$)

Δh : Difference in specific enthalpy at any level between the disturb-
ance and environment [$c_p (T_{dis} - T_e)$]

H: Rate of heating per unit mass at any pressure level

H_r : Rate at which latent heat of condensation is released from low-level water vapor convergence and made available for enthalpy increase

H_c : Rate at which heat is used by the ascending cloud air to warm itself up to the temperature of the environment

H_s : Net sensible heating rate due to the release of latent heat from low-level water vapor convergence ($H_r - H_c$)

H_u : Cooling rate produced inside an elemental cylindrical section by ascent initiated at upper levels (above cumulus cloud base)

H_{net} : Net warming rate from condensation at any time period ($H_s + H_u$)

H_o : Rate of heat lost by divergent mass outflow from an elemental cylindrical section

H_{adv} : Rate of heat advection (or ventilation) out of an elemental cylindrical section

H_{rad} : Rate of heating from radiation

F: Specific fractional rate of apparent cooling at any pressure level (percentage reduction of sensible heat per unit time)

F_v : Fractional apparent cooling rate due to ventilation

F_{div} : Fractional apparent cooling rate due to divergent outflow

F_{net} : Net apparent fractional cooling rate ($F_v + F_{div}$)

ϕ : Fraction of the incoming low-level mass per millibar that reaches a particular pressure level

Only a small portion of the latent heat contained in the converging water vapor is, however, available for warming the disturbance.

Firstly, not all the vapor will condense. Mixing with non-cloud air will occur and part of the moisture will go into increasing the humidity of the environment.

Secondly, part of the heat of condensation will be used for expansion work and in increasing the potential energy of the parcels.

These portions of the released condensation heat are not available for sensibly warming the disturbance.

Thirdly, before the ascending cloud air can raise the temperature of the disturbance, it must itself be raised up to the temperature of the ambient air from the temperature that would result from dry adiabatic ascent. The heat used to achieve this is not available for sensible warming of the disturbance.

The maximum amount of sensible heat resulting from condensation of the converging low-level water vapor is thus much reduced by virtue of mixing, expansion, and lifting. Of the residue, only that part which gives the cloud air an excess temperature above that of the cloud-free environment can be utilized to raise the temperature of the system. As will be shown below, the maximum amount of latent heat that can be used for sensible temperature increase is only 10 percent of the heat contained in the low-level water vapor convergence. This small percentage of available water vapor for

sensible heating is of crucial importance and has not been given complete consideration in the mathematical models of storm development referred to above.

The rate of low-level mass convergence into the 3° radius disturbance due to convergence under cloud base is given by:

$$\frac{dM_i}{dt} \doteq - \int_{V \text{ (sub-cloud)}} \rho \nabla_2 \cdot \mathbf{w} dV \doteq - \overline{(\nabla_2 \cdot \mathbf{w})} A_{\text{hor}} \frac{\Delta p}{g} \quad (1)$$

where the symbols in this and subsequent equations are defined in Table 1. Cloud base is assumed to occur at 950 mb and so Δp is approximately 60 mb. As the divergence of the wind is one of the most difficult parameters to compute from synoptic data, care was taken to consider all available surface wind values. All available ship and land station reports were used. Wind reports were broken into radial and tangential components. Surface divergence was calculated in a polar coordinate grid. The average computed convergence in a 3° radius for each case is shown in Fig. 23. Over the comparable four time periods the developing case indicates a convergence almost two times higher than the non-developing case. We assume that this convergence is typical of the sub-cloud layer (surface to 950 mb).

Not all of the moisture contained in this air mass will be condensed, however. Only a fraction of the air coming into the system at low levels will rise all the way to the top of the troposphere in cumulonimbus clouds and condense all its water vapor. The rest

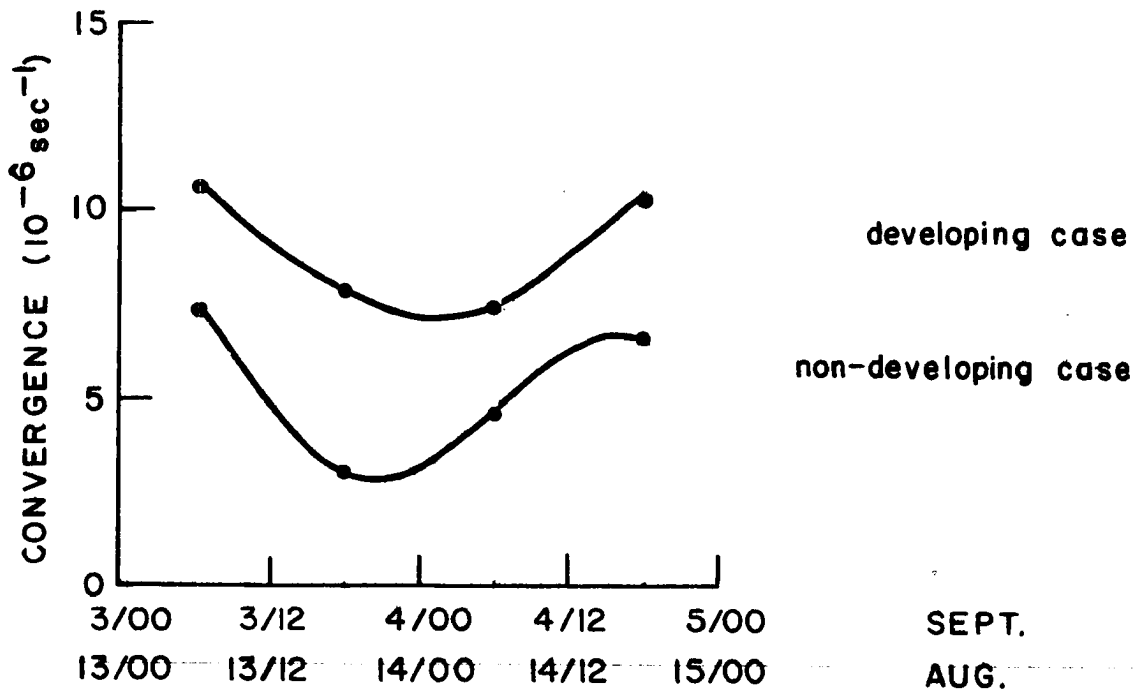


Fig. 23. Average 12 hour overlapping surface convergence with time in a 3° radius around the two storms. The assumed convergence centers are indicated by solid dots in Figs. 9 and 11.

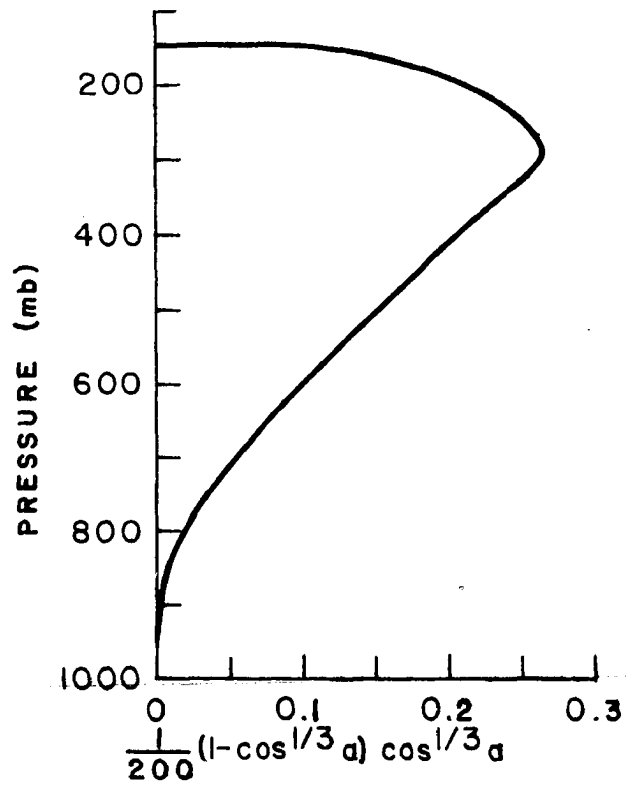


Fig. 24. Assumed fraction of the mass arising from the sub-cloud layer which terminates in 100 mb layers centered at a particular pressure level.

will raise to lower heights according to the width of the updraft and entrainment characteristics of the ascending current. For this reason only a fraction of the latent heat initially contained in the low-level convergence (potential heat) will actually be released.

In order that quantitative computations can be made it will be assumed that Gray's (1967a) representation of three sizes of cumulus clouds occurring in equal area amounts are typical for both cases. These three sizes of cumulus clouds are:

1. small cumuli (Cu) which extend from 950 to 700 mb
2. towering cumuli (TWG Cu) which extend from 950 to 500 mb with maximum upward speed twice the updraft velocity of the small cumuli
3. cumulonimbi (Cb) which extend up to 200 mb with maximum updraft velocities twice as large as the towering cumuli updrafts

The convergence under cloud base is assumed to be channeled into cumulus convection of these three sizes. Assuming an equal relative areal distribution of these three sizes of cumulus updrafts, then about one-third of the low-level mass inflow will not penetrate to levels above 500 mb. The sub-cloud air will ascend to various heights according to the entrainment character of the raising current. For the purpose of this simple model, the fraction of the incoming low-level mass per millibar that reaches a particular pressure level is taken to be given by:

$$\phi(p) = \frac{1}{200} (1 - \cos^{1/3} a) \cos^{1/3} a \quad (2)$$

where $a = \left(\frac{950 - p}{800}\right) \pi/2$. A graphic portrayal of this function is shown in Fig. 24. Table 2 (Column B) shows the fractional values of $\phi(p)$ per 100 mb intervals. A similar function has previously been used by Gray (op. cit.) to specify the wind eddies produced by cumulus updrafts and downdrafts in a hurricane environment.

The amount of lower level mass reaching a particular level per unit time per millibar thickness is given by $\phi(p) \frac{dM_i}{dt}$. Parcels that lose their buoyancy and mix at lower pressure level will only release a fraction of their available water vapor, or $\frac{q_o - q_s(p)}{q_o}$ where $q_s(p)$ is the saturation specific humidity at the mixing level and q_o is the surface specific humidity. This ratio is portrayed in Column A of Table 2. The actual rate of acquisition of condensation heat of the parcel per millibar thickness per gram at any pressure level from the converging low-level water vapor is then given by:

$$\phi(p) q_o L \left(\frac{q_o - q_s(p)}{q_o} \right) \frac{dM_i}{dt}$$

where L is the latent heat of condensation.

TABLE 2

Computation of the heat of condensation available for warming of a disturbance's atmosphere from sub-cloud layer convergence. Values are averages for 100 mb layers centered at the pressure levels indicated.

P (mb)	A $\frac{q_0 - q}{q_0}$	B $\phi(p)$	C $E(p)$	D $\frac{q_0 - q \phi(p) E(p)}{q_0}$	E ΔT_a	F $\frac{c_p \Delta T_a \phi}{q_0 L}$	G Comb. Effect.
200	1.00	0.21	0.70	0.15	37.2	0.13	0.02
300	0.91	0.25	0.77	0.18	30.0	0.15	0.03
400	0.78	0.21	0.81	0.13	26.8	0.10	0.03
500	0.63	0.15	0.86	0.08	21.9	0.07	0.01
600	0.49	0.10	0.90	0.04	16.8	0.03	0.01
700	0.34	0.06	0.96	0.02	12.7	0.02	0.00
800	0.21	0.02	0.98	0.00	8.5	0.00	0.00
900	0.09	0.00	1.00	0.00	4.3	0.00	0.00
TOTAL		1.00		0.60		0.50	0.10

(Overall efficiency of cumulus convection: $0.60 - 0.50 = 0.10$)

- A. Fraction of the original water vapor converging into the disturbance at sub-cloud layers which is condensed in or below 100 mb layer of consideration.
- B. Fraction of ascending sub-cloud air which terminates in individual 100 mb pressure layers [assuming Gray's (1967a) cumulus mixing values Fig. 24].
- C. Fraction of the released heat of condensation which is used to raise the enthalpy of the ascending air from that which would occur with dry adiabatic ascent. The rest of the heat goes into increasing the potential energy above what it would have with dry adiabatic ascent.
- D. Combined products of A, B, and C. Fraction of the total latent heat contained in the low-level convergence that will be used at individual levels to raise the enthalpy of the cloud air above that of dry adiabatic ascent.
- E. Temperature difference in ° C between the hurricane season tropical atmosphere and the equivalent dry adiabatic temperature for ascent from 950 mb.
- F. Fraction of the total latent heat contained in the low-level moisture convergence that will be used in raising the cloud air to the temperature of the environment.
- G. Difference between D and F or percentage of low-level water vapor convergence which goes to raise the enthalpy in each 100 mb layer (H_S). The integrated value of this column shows that only 10 percent of the low-level water vapor convergence is actually utilized for increasing the enthalpy of the system.

Only a small part of this condensation heat acquisition can be used to increase the enthalpy of the air. A large fraction will be used for potential energy increase. For a parcel raised moist adiabatically to a certain level p , the first law of thermodynamics gives:

$$\int_{p_0}^p Ldq_s = \int_{p_0}^p c_p dT_{\text{moist}} - \int_{p_0}^p \alpha(p)_{\text{moist}} dp \quad (\text{moist ascent}) \quad (3a)$$

$$0 = \int_{p_0}^p c_p dT_{\text{dry}} - \int_{p_0}^p \alpha(p)_{\text{dry}} dp \quad (\text{dry ascent}) \quad (3b)$$

where q_s is the saturation specific humidity and α is the specific volume of the air. The percentage ratio of total condensation heat which is used to increase the enthalpy of the cloud air above the enthalpy of a dry adiabatic sounding, is given by subtracting (3b) from (3a):

$$E(p) = c_p(T_{\text{moist}} - T_{\text{dry}})_p \bigg/ \int_{p_0}^p Ldq_s = 1 - \left(\frac{\int_{p_0}^p (\alpha_{\text{moist}} - \alpha_{\text{dry}}) dp}{\int Ldq_s} \right) \quad (4)$$

Column C of Table 2 gives this fraction for 100 mb layers centered at the specified pressure levels for an assumed surface mixing ratio of 20 g/kg. The rest of the condensation heat (0 to 30 percent) goes to increasing the potential energy p_0 of the parcel [i. e. $\int (\alpha_{\text{moist}} - \alpha_{\text{dry}}) dp$] above the potential energy it would have with dry adiabatic ascent. The rate at which heat is made available from condensation for enthalpy increase per unit mass per millibar thickness at any pressure level is finally:

$$H_r(p) = \phi(p)q_0 L \frac{(q_0 - q_s(p))}{q_0} E(p) \frac{dM_i}{dt} \quad (5)$$

The combined coefficient of potential enthalpy increase above dry adiabatic parcel ascent per 100 mb for the rising parcel is

indicated in Column D of Table 2. It can be seen that reduced condensation from entrainment or mixing and potential temperature increase reduce the amount of latent heat available for increase of enthalpy to approximately 60 percent of the amount available from the low-level water vapor convergence.

In addition, it should be recognized that of this amount only a small portion representing the excess enthalpy of the cloud over the environment will provide a heat source for tropospheric warming. The air reaching any pressure level will use up the major part of its latent heat to raise its enthalpy from that of a dry adiabatic expansion to the enthalpy of the environment. This further heat extraction rate per gram is given by:

$$H_c(p) = \phi(p) c_p (T_{ce} - T_{dry}) p \frac{dM_i}{dt} \quad (6)$$

where T_{ce} is the temperature at any level of the air surrounding the cumulus and T_{dry} is the temperature at any level that would have resulted from dry adiabatic ascent from 950 mb. This large fraction of released condensation heat which produces parcel warming from a dry adiabatic environment to the tropical storm environment cannot be utilized for sensible heat increase. Only the excess enthalpy of the cloud air above that of the environment constitutes a source of cumulus induced sensible heat increase.

Column E lists the temperature difference at each pressure level between the dry adiabatic ascent from 950 mb and the temperature of the environment at that level.

The actual sensible heating rate (H_s) at any pressure level due to latent heat release of sub-cloud layer water vapor convergence is thus given by:

$$H_s(p) = H_r(p) - H_c(p) \quad (7)$$

$H_s(p)$ is small in comparison with both $H_r(p)$ and $H_c(p)$.

Column F of Table 2 lists the fraction of the potential latent heat contained in the sub-cloud layer mass inflow which is required in each 100 mb layer to raise the cloud parcels to the temperature of the ambient air. The difference between Column D (condensation heat warming) and Column F gives the net sensible warming efficiency of the process for each 100 mb layer. This net warming efficiency is shown in Column G. Integrating through the troposphere one sees that only 10 percent of the potential latent heat contained in the low-level inflow can be utilized for sensible warming of the troposphere. This is a very low percentage indeed. The partition of the potential heat into the different categories of Table 2 is shown graphically in Fig. 32.

Fig. 25 portrays the calculated vertical profiles of average 12 hour sensible warming $\frac{(H_s) \Delta t}{c_p}$ per unit mass for the developing and non-developing disturbances. The developing case had twice as much sensible warming per 12 hours.

Convergence above cloud base. As shown in Figs. 20 and 21, convergence above 900 to 850 mb produces sensible cooling of the disturbance. The amount of sensible cooling depends on the magnitude of the upper level convergence. The actual sensible cooling

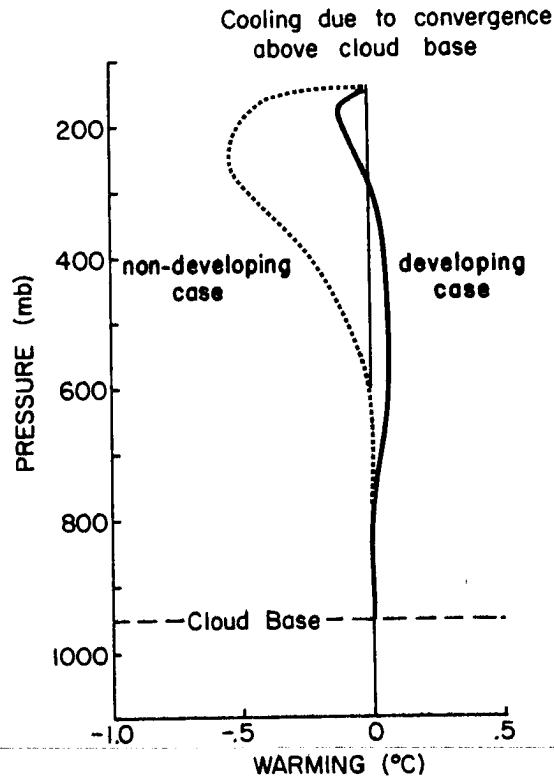


Fig. 26. Average warming per 12 hours resulting from ascents initiated by convergence above 950 mb, as indicated in Figs. 12 and 13. Averages were taken over the 48 hours considered for both cases. Solid line is for the developing case. These warming profiles correspond to the average value of $\frac{H_u \Delta t}{c_p}$ per unit mass.

disturbance air is then replaced by surrounding environmental air of lower temperature. This ventilation of the disturbance depends on the magnitude of the vertically integrated relative wind and on the disturbance-environment temperature difference. The vertical wind shears between 200 and 850 mb provide a good estimate of this ventilation effect. The ventilation of heat out of the disturbance can occur with zero divergence.³

Consider an elemental cylindrical section at any level p . The average temperature of the elemental volume is assumed to be T_{dis} and the mean air density ρ . Let the mean temperature of the environment outside the disturbance area at the same pressure level be T_e . The excess enthalpy of the elementary cylindrical section per unit mass is then $\Delta h(p) = c_p (T_{dis} - T_e)$. Consider the relative wind $\mathbf{v}_r(p)$ at any pressure level flowing through the elemental section. This wind will be given by $\mathbf{v}_r(p) = \mathbf{v}(p) - \mathcal{C}$ where $\mathbf{v}(p)$ is the actual wind at any pressure level and \mathcal{C} is the movement of the disturbance. The rate of heat advection per unit mass through the lateral area A_{lat} of this section (Fig. 22) at any pressure level is given by:

$$H_{adv}(p) = \frac{\int \mathbf{v}_r(p) \cdot \nabla[\rho \Delta h(p)] dV}{m} = \frac{\int A_{lat} \rho \Delta h(p) \mathbf{v}_r(p) \cdot d\mathbf{A}}{m} = \frac{|\mathbf{v}_r(p)| \Delta h(p)}{m} \frac{2R\Delta p}{g}$$

or

$$H_{adv}(p) = \frac{2|\mathbf{v}_r(p)| \Delta h(p)}{R\pi} \quad (8)$$

³Riehl and Malkus (1961) have shown that in the latter stages of development of hurricane Daisy (1958) the convergent circulation through the storms at middle levels (lateral inflow) acted to bring air of lower energy content into the system. This acted as a constraint to the intensification of the storm. They referred to this type of cooling effect from the middle-level convergence as "ventilation". In an incipient disturbance, however, when the temperature gradients between the environment and the disturbance are small, this type of cooling has been calculated to be negligible. We have reserved the term "ventilation" only for the non-divergent advection of heat due to the wind flow relative to the moving disturbance.

where $V (\pi R^2 \Delta z)$ and $m (\pi R^2 \frac{\Delta p}{g})$ are the volume and mass of the elemental section, $A = 2R\Delta z$, and $|\mathbf{v}_r(p)|$ is the absolute magnitude of the relative wind vector at any level. The fractional rate of advection of mass out of the disturbance at any level due to ventilation ($F_v(p)$) is then given by:

$$F_v(p) = \frac{2|\mathbf{v}_r(p)|}{R\pi} \quad (9)$$

The fraction of disturbance mass exchange at any level by this ventilation effect acting during a time interval Δt is thus $F_v(p)\Delta t$.

This fractional ventilation cooling was computed every twelve hours from the actual wind values in 100 mb layer increments from 950 to 150 mb. The 12 hour average ventilation factors for the four time intervals considered in each case is shown in Fig. 27. Maximum ventilation (or apparent cooling) takes place at 200 mb. This net cooling effect is three times larger in the non-developing case.

Divergent outflow at upper levels. In addition to the inhibitory ventilation outflow relative to the disturbance, divergent mass outflow also acts to carry away part of the accumulated condensation heat. This heat transport by the mass divergence can occur with zero ventilation. Fig. 12 shows that the divergent outflow is confined to a very shallow layer near 200 mb.

The rate of heat loss by divergent outflow at any level from an elemental cylinder section per unit mass is:

$$\begin{aligned} H_o(p) &= \frac{1}{m} \int_V \rho \Delta h(p) \nabla_2 \cdot \mathbf{v}(p) dV \\ &= \Delta h(p) \overline{\nabla_2 \cdot \mathbf{v}(p)} (\pi R^2 \frac{\Delta p}{g}) / \pi R^2 \frac{\Delta p}{g} = \Delta h(p) \overline{\nabla_2 \cdot \mathbf{v}(p)} \end{aligned} \quad (10)$$

The fractional cooling rate due to divergent outflow is thus given by:

$F_{\text{div}}(p) = \overline{\nabla_2 \cdot \mathbf{v}(p)}$. This heat divergence was computed in twelve hour intervals in layers of 100 mb from 950 to 150 mb for the four observation times under consideration. The average results are shown in Fig. 27. The effect is negligible except in a shallow layer around 200 mb.

Computation of Net Warming

The various warming effects (H_r , H_c , and H_u , etc.) were added together to obtain H_{net} for each twelve hour period and the cooling influence terms (F_v and F_{div} , or F_{net}) were applied to a single warming parameter. To the net warming ($\frac{H_{\text{net}}}{c_p} \Delta t$) obtained in the first twelve hour interval the first heating reduction coefficient ($1 - F_{\text{net}}$) was applied. This gave the net twelve hour residual heating. This residual heating was added to the condensation warming during the next twelve hours and a second cooling factor was applied and so on for each of the four 12 hour periods of consideration. This procedure was applied to each of the 100 mb intervals between 950 and 150 mb. The cumulative heating for the intervals $n = 1$ to $n = 4$ for any pressure level by this method is given by:

$$\Delta T_{\text{dis}} = \sum_{n=1}^4 \frac{(H_{\text{net}})_n}{c_p} \Delta t \prod_{j=n}^4 (1 - F_{\text{net}}^j) \quad (11)$$

where H_{net} is the net heating (resulting from sub-cloud plus upper-level convergence, $H_s + H_u$) and F_{net}^j is the net percentage cooling factor (ventilation plus outflow effects, $F_v + F_{\text{div}}$) for the j th time

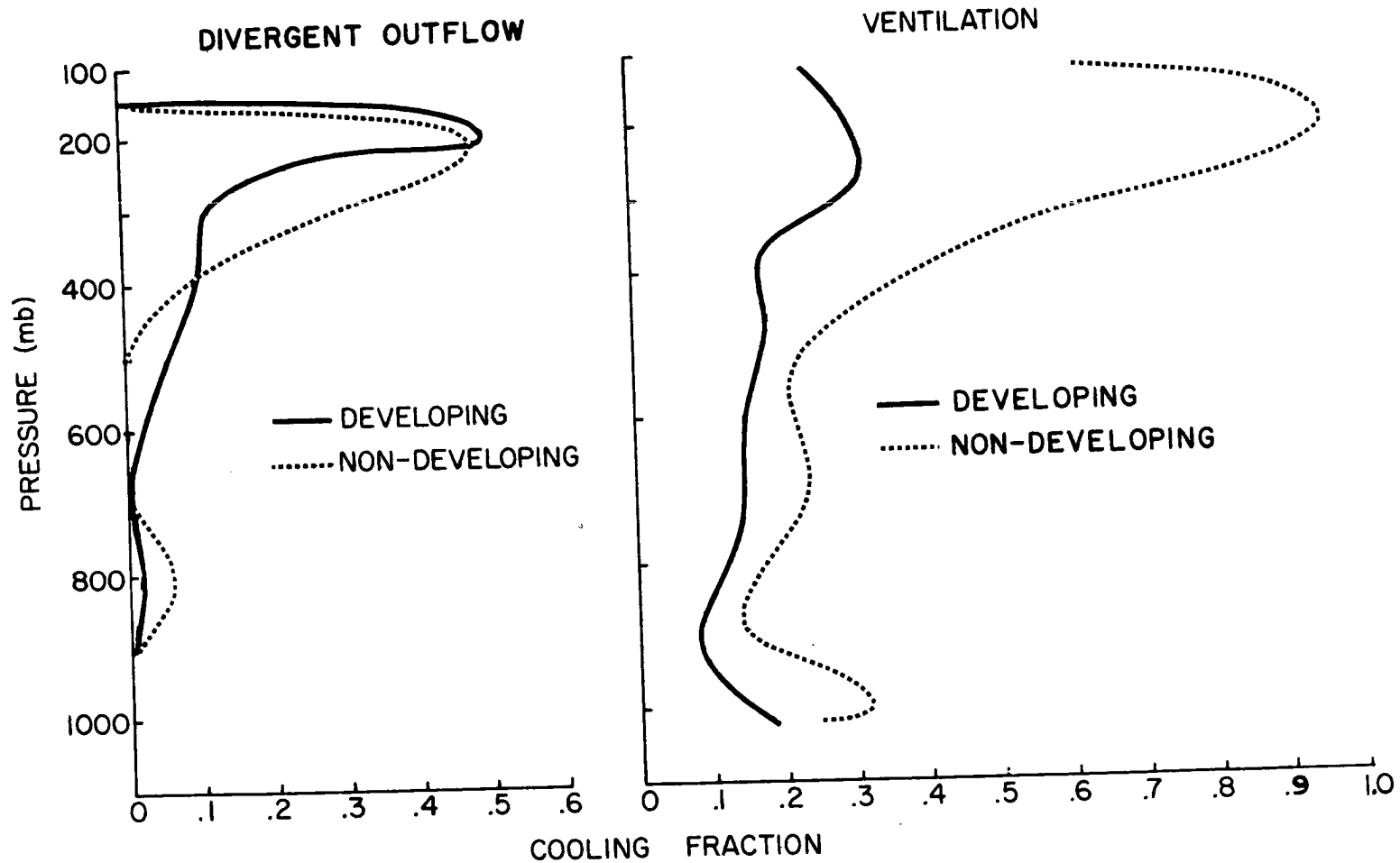


Fig. 27. Fraction of the heat of condensation carried away from the system (or apparent cooling) by the outflow and ventilation mechanisms per 12 hours. Averages were computed over the 48 hour period of consideration. These profiles correspond to the average value of $F_{div}(p)$ and $F_v(p)$ respectively.

interval, ΔT_{dis} is the accumulated increase in temperature at the end of the period and Δt equals 12 hours.

The equivalent tropospheric heating within a 3° radius above the cloud base at the various time periods is shown in Fig. 28. For the development case the mean tropospheric warming within the disturbance was 0.45° C. No warming was obtained in the non-development case. Zero initial temperature anomalies were assumed. This net heating difference is a reflection of the smaller surface convergence, greater middle-level convergence, and much greater ventilation in the non-developing disturbance. The large ventilation in the non-developing case actually prevented it from cooling more than it did.

The actual magnitude of this mean two-day tropospheric warming in the development case is, however, too small. The mean surface pressure (inside a circular area of 3° radius around the developing disturbance center) was observed to drop by no less than 5 mb during this 48 hour interval. The pressure drop at the surface resulting from a uniform tropospheric warming of 1° C, can be computed from hydrostatic considerations to be but 3 to 4 mb. The computed tropospheric warming of 0.45° C would produce at most a 2 mb mean pressure drop. The computed warming was thus only about 40 percent of the actual warming.

Previous models of hurricane development have incorporated condensation heat but have not in general incorporated cooling constraints such as ventilation, divergent outflow, and middle-level ascent. One of the problems in hurricane modeling

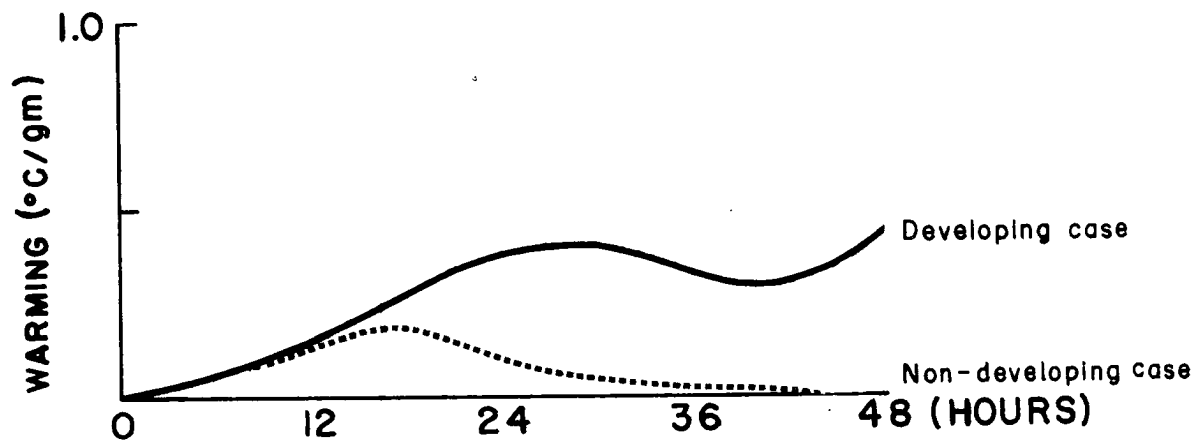


Fig. 28. Average warming of the troposphere above cloud base with time, 950 to 150 mb. A 1° C warming is equivalent to about a 3½ mb surface pressure drop.

has been to find conditions which restrain growth. When these realistic constraints were introduced in the cases considered in this study, development from condensation alone was not possible.

One of the main discrepancies between the numerical models proposed in the past and the computations performed in this study lies in the way the release of latent heat is incorporated. Although there have been attempts (Ooyama, 1963; Charney and Eliassen, 1964; Ogura, 1964; Syōno and Yamasaki, 1966) to incorporate the reduction of the latent heat by entrainment and mixing, these models, in general, do not take into account the fact that only that enthalpy of the cumulus parcel in excess of the environment can be utilized for warming. Kuo (1965), on the other hand, incorporates most of these latter restrictions but neglects the losses through mixing.

In view of the failure of the latent heat source to account for all the observed warming in the early intensifying stages, one should look for other possible heat sources. A significant contribution might be accomplished by the trapping of radiation by the cloud canopies over the incipient disturbance.

To test this possibility, we assumed that the cloud canopies trap approximately one-third of the daily outgoing infrared radiation. Typical infrared losses per day in the summertime tropical atmosphere are equivalent to a mean tropospheric cooling of approximately 1.5° C (London, 1957). This value has been

roughly verified by Riehl (1962) for the Caribbean Sea in autumn. We will now assume a relative increase in the tropospheric temperature between the disturbance and its environment of 0.25° C per 12 hours due to this trapping of infrared radiation by the cloud canopies. The assumed distribution with height of the mean tropospheric warming of 0.25° C per 12 hours is portrayed in Fig. 29. For convenience we chose to distribute this net tropospheric radiation warming with the same function of Eq. (2).

This assumed radiation heat source was incorporated into the model and the heat budget performed again. No further detailed consideration of the radiational influence was attempted. The resulting individual vertical temperature profiles from all warming sources including radiation are portrayed in Fig. 30, and the net mean tropospheric warming in Fig. 31. With the addition of the radiation heating the computed warming now corresponds to about 4 mb pressure drop. This comes closer to the observed pressure fall of 5 mb. To obtain complete correspondence between observed and calculated warming, we would have to assume that the cloud canopies above the disturbance trap slightly more than one-third of the infrared losses in comparison with the environment.

More studies of the radiation balance of tropical disturbances may have to be made before a complete understanding of the thermodynamics of tropical storm development is obtained.

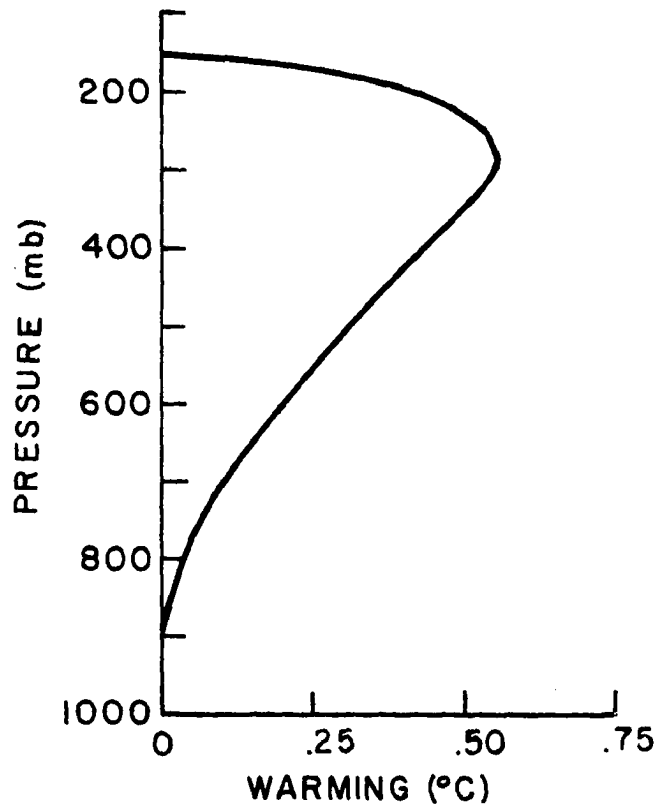


Fig. 29. Distribution with height of relative tropospheric warming resulting from an assumed differential trapping of infrared radiation between the disturbance and its environment which leads to a mean relative tropospheric rise in temperature of the disturbance over its environment of 0.25°C per 12 hours.

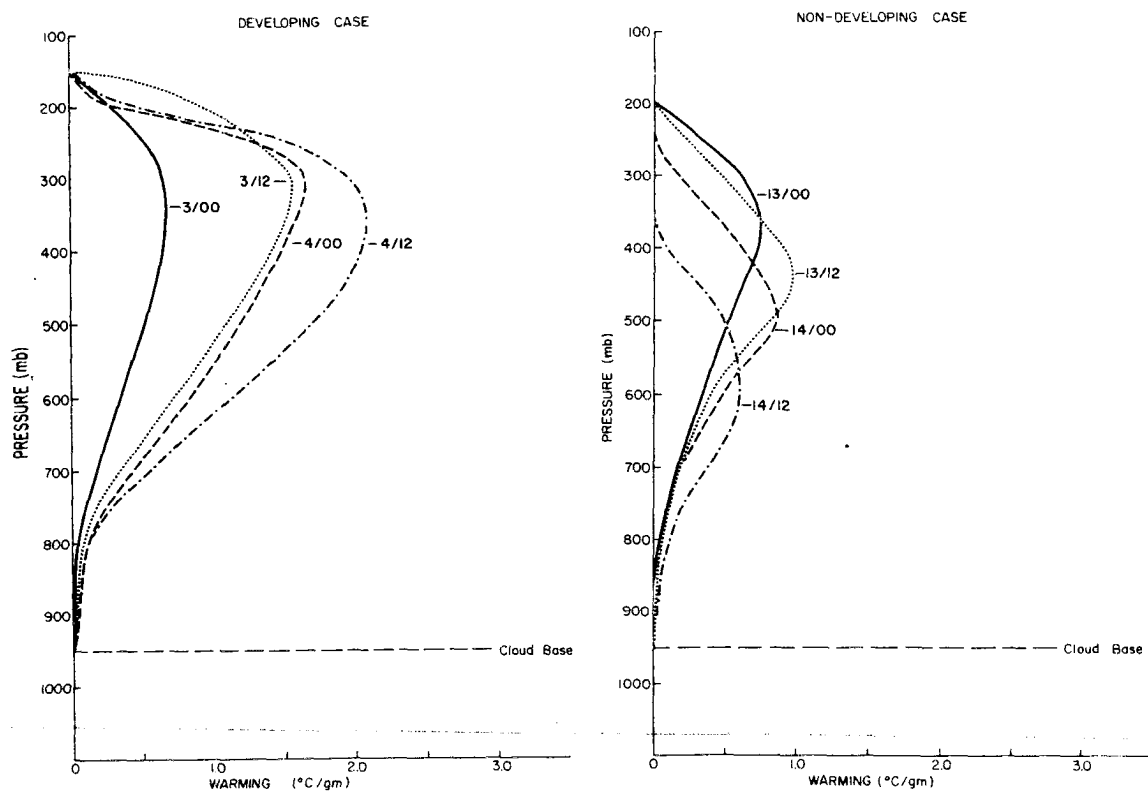


Fig. 30. Calculated resultant temperature anomaly profiles for the times indicated. Anomalies are taken from the Swan Island mean August sounding. All heating effects, including radiation, have been included.

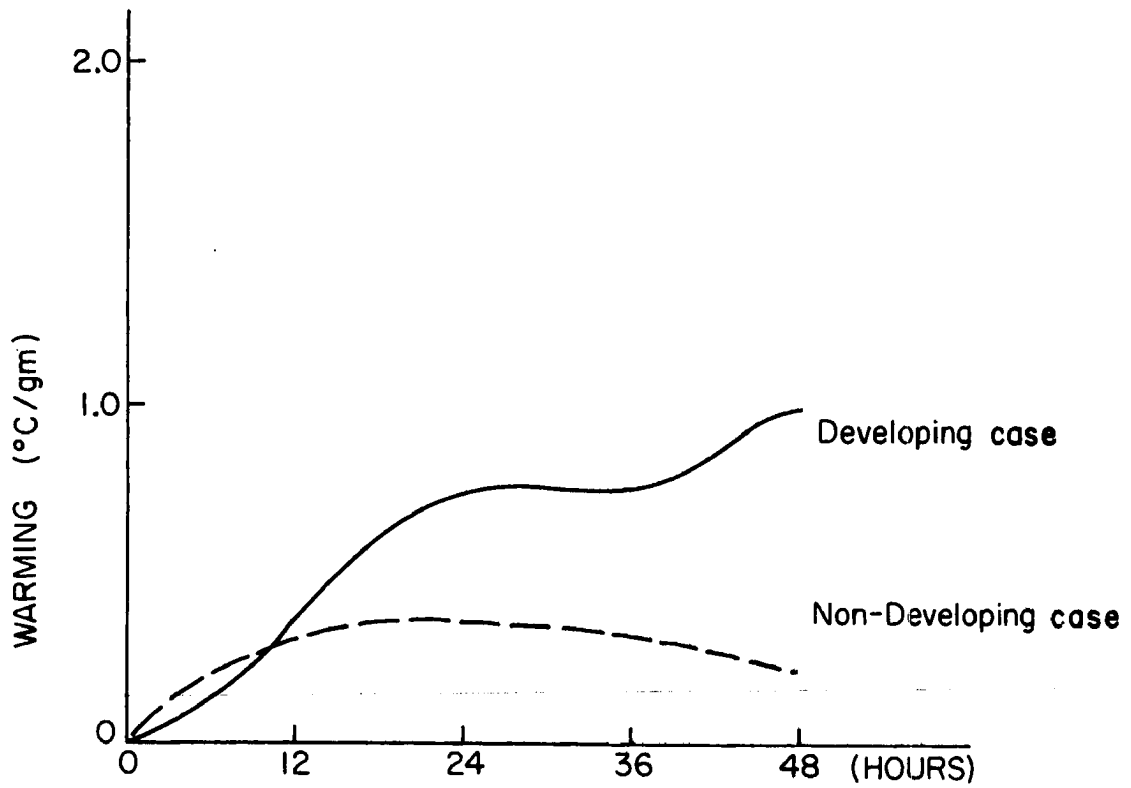


Fig. 31. Equivalent uniform warming of the troposphere above cloud-base with time, 950 to 150 mb, radiation effects included. A 1° C warming is equivalent to about 3½ mb surface pressure drop. Mean pressure decrease over the 3° radius in the development case was 5 mb.

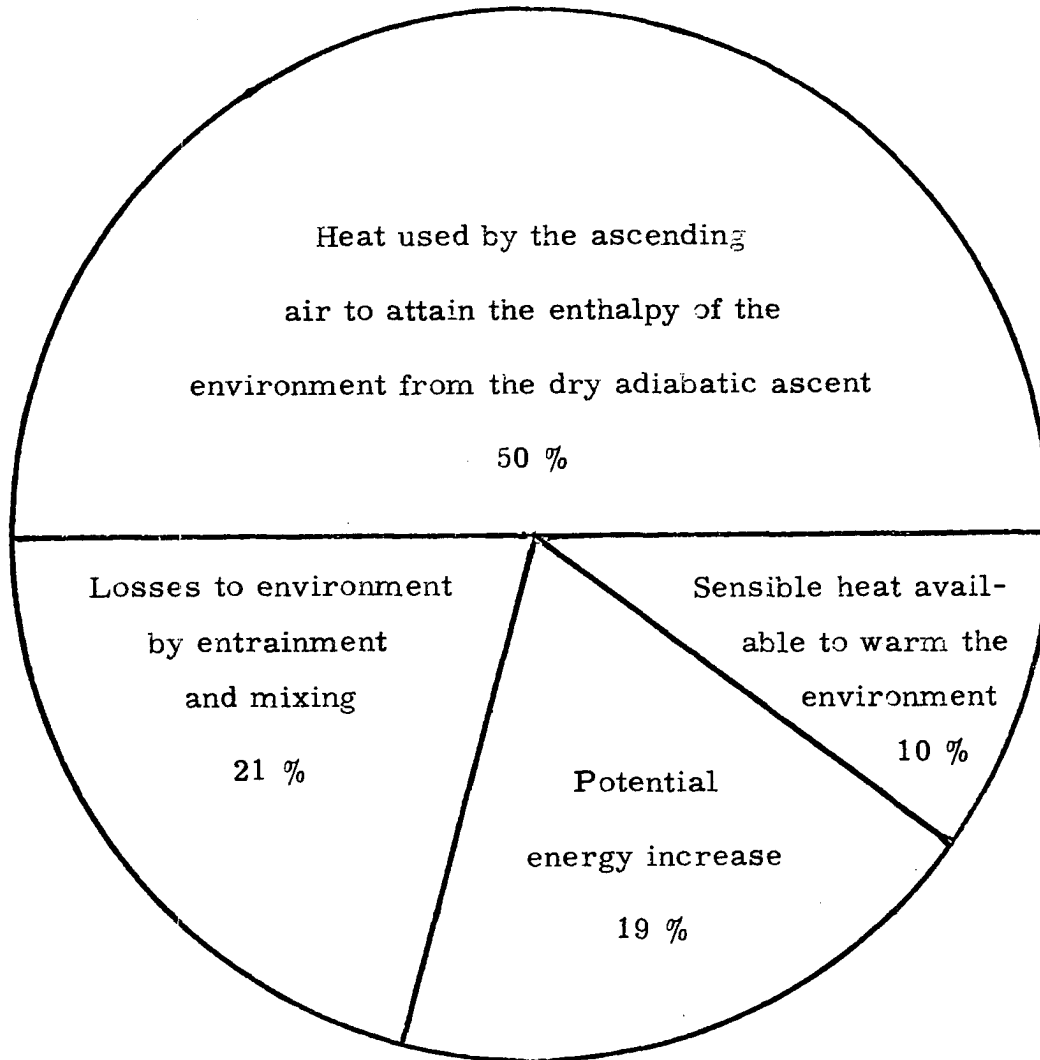


Fig. 32. Utilization of the latent heat contained in the sub-cloud layer inflow.

VI CONCLUSIONS AND FINAL REMARKS

It has been shown that the intensification potential of two similar appearing tropical disturbances can be very different. A careful study of the two cases indicates differences which are of critical importance in tropical storm development. The convergence under the base of the cumulus clouds in the developing disturbance is twice as large as the low-level convergence in the non-developing case. But this was only one of the potential development differences. The inhibitory effect of ventilation was three times greater in the non-developing than in the developing case. With the greater cooling due to larger middle level convergence in the non-developing case, a four to fivefold advantage in potential heat accumulation was observed between the two cases.

The importance of low-level water vapor convergence as a heating source was closely examined. It is shown that only 10 percent of the potential latent heat contained in the converging sub-cloud layer can be utilized to increase a disturbance's tropospheric temperature. When, to this already small source of potential warming, we apply the cooling effects of ventilation, divergence, and middle-level convergence, we realize how difficult it is to initially increase the mean tropospheric temperature of a tropical disturbance above that of the environment.

When this 10 percent warming efficiency is included, the typically observed surface water vapor convergences of tropical disturbances always prove deficient in explaining the required warming for initial vortex development.

Table 3 shows the maximum tropospheric warming and corresponding hydrostatic surface pressure drops attained in one day from various sub-cloud layer convergences and without inclusion of cooling processes. This warming is insufficient to account for the initial typical observed deepening of intensifying disturbances.

This general failure of the cumulus convection to provide the necessary initial tropospheric heating for early disturbance intensification indicates that there must be another source of heating. For instance, a significant contribution to early disturbance development may be accomplished by the trapping of ultraviolet and infrared radiation by the cloud canopies developed above the incipient disturbance. If this does, in fact, prove to be a realistic contribution, then the primary role of cumulus convection in early disturbance growth will be the indirect one of generating this radiation shield, rather than the direct one of providing the condensation. A more precise determination of the radiation contribution would appear to be a highly beneficial future research endeavor. The assumed one-third trapping of infrared radiation by the cloud canopies is a conservative estimate based on discussion with a number of radiation specialists.

VI CONCLUSIONS AND FINAL REMARKS

It has been shown that the intensification potential of two similar appearing tropical disturbances can be very different. A careful study of the two cases indicates differences which are of critical importance in tropical storm development. The convergence under the base of the cumulus clouds in the developing disturbance is twice as large as the low-level convergence in the non-developing case. But this was only one of the potential development differences. The inhibitory effect of ventilation was three times greater in the non-developing than in the developing case. With the greater cooling due to larger middle level convergence in the non-developing case, a four to fivefold advantage in potential heat accumulation was observed between the two cases.

The importance of low-level water vapor convergence as a heating source was closely examined. It is shown that only 10 percent of the potential latent heat contained in the converging sub-cloud layer can be utilized to increase a disturbance's tropospheric temperature. When, to this already small source of potential warming, we apply the cooling effects of ventilation, divergence, and middle-level convergence, we realize how difficult it is to initially increase the mean tropospheric temperature of a tropical disturbance above that of the environment.

TABLE 3

Sub-cloud layer convergences with resulting mean warming between 950 and 150 mb and corresponding surface pressure falls per day under assumed surface mixing ratio of 20 gm/kgm, and a 10 percent efficiency for cumulus induced warming. No cooling due to ventilation, divergent outflow, or middle-level convergence was assumed.

<u>Sub-cloud Layer Convergence</u>	<u>$\Delta T/\text{day}$</u>	<u>$\Delta p/\text{day}$</u>
10^{-6} sec^{-1}	.04° C	.2 mb
$5 \times 10^{-6} \text{ sec}^{-1}$.22° C	.9 mb
10^{-5} sec^{-1}	.45° C	1.8 mb

ACKNOWLEDGMENTS

The author wishes to express his sincere gratitude to Dr. William Gray under whose guidance this investigation was performed. He suggested the problem and patiently supervised all phases of the research. His kind criticism and encouragement is very much appreciated. We are indebted to Dr. Michio Yanai for the use of his objective analyses program and to Mr. Bruce Mendenhall for his participation in the data collection and actual running of the computer program. We also want to thank the National Hurricane Research Project and the San Juan Weather Bureau for furnishing the aircraft and synoptic data utilized in this investigation. Thanks are also due to Mrs. Janice Piper for patiently typing this report.

This research has been jointly sponsored by the National Science Foundation under the U. S. -Japan Joint Cooperative Science Program and by the Environmental Science Services Administration.

REFERENCES

- Alaka, M. A., 1958: Dynamics of upper air outflow in hurricanes. Geophysics, 6, 133-146.
- _____, 1963: Instability aspects of hurricane genesis. National Hurricane Research Project Report No. 64.
- Charney, J. G., and A. Eliassen, 1949: A numerical method for predicting the perturbations of the middle-latitude westerlies. Tellus, 1, 38-54.
- _____, 1964: On the growth of the hurricane depression. Journal of Atmospheric Science, 21, 68-75.
- Colón, J. A., and W. R. Nightingale, 1963: Development of tropical cyclones in relation to circulation patterns at 200 mb level. Monthly Weather Review, 91, 329-336.
- Fett, R. W., 1964: Aspects of hurricane structure: new model considerations suggested by TIROS and Project Mercury observations. Monthly Weather Review, 92, 43-60.
- _____, 1966: Upper-level structure of the formative tropical cyclone. Monthly Weather Review, 94, 9-18.
- Gray, W. M., 1967a: The mutual variation of wind shear, and baroclinicity in the cumulus convective atmosphere of the hurricane. Monthly Weather Review, 95, 55-73.
- _____, 1967b: Global view of the origin of tropical disturbances and storms. Atmospheric Science Research Report No. 114, Colorado State University.
- Hawkins, H. F., et al., 1962: Inventory, use and availability of National Hurricane Research Project data gathered by aircraft. National Hurricane Research Project Report No. 52.
- Jordan, C. L., 1957: A mean atmosphere for the West Indies area. National Hurricane Research Project Report No. 6.
- Krishnamurti, T. N., and D. Baumhefner, 1966: Structure of a tropical disturbance based on solutions of a multi-level baroclinic model. Journal of Applied Meteorology, 5, 396-406.

REFERENCES continued

- Kuo, H. L., 1965: On formation and intensification of tropical cyclones through latent heat release by cumulus convection. Journal of Atmospheric Science, 22, 40-63.
- London, J., 1957: A study of the atmospheric heat balance, Final Report. Contract No. AF 19(122)-165, New York University.
- Ogura, Y., 1964: Frictionally controlled thermally driven circulation in a circular vortex with application to tropical cyclones. Journal of Atmospheric Science, 21, 610-621.
- Ooyama, K., 1963: A dynamical model for the study of tropical cyclone development. Department of Meteorology and Oceanography, New York University. Presented at the 43rd Annual Meeting of American Meteorological Society, 1963.
- Riehl, H., 1945: Waves in the easterlies and the polar front in the tropics. Department of Meteorology, University of Chicago Miscellaneous Report 17, 79 pp.
- _____, 1948a: On the formation of West-Atlantic hurricanes. Miscellaneous Report No. 24, Part 1, Dept. of Meteorology, University of Chicago.
- _____, 1948b: On the formation of typhoons. Journal of Meteorology, 5, 247-264.
- _____, 1950: A model of hurricane formation. Journal of Applied Physics, 21, 917-925.
- _____, 1962: Radiation measurements over the Caribbean during the autumn of 1960. Journal of Geophysical Research, 67, 3935-3942.
- Riehl, H. and J. Malkus, 1958: On the heat balance in the Equatorial Trough Zone. Geophysica, 6, 503-538.
- _____, 1961: Some aspects of hurricane Daisy, 1958. National Hurricane Research Project, Report No. 46.
- Sadler, J., 1963: Tiros observations of the summer circulation and weather patterns of the eastern North Pacific. University of Hawaii Scientific Report No. 5, 47 pp.

REFERENCES continued

- Syōno, S., 1962: A numerical experiment of the formation of tropical cyclones. In Proceedings of the International Symposium on Numerical Weather Prediction in Tokyo. The Meteorological Society of Japan, Tokyo.
- Syono, S. and M. Yamasaki, 1966: Stability of symmetrical motions driven by latent heat release by cumulus convection under the existence of surface friction. Journal of Meteorological Society, Japan, 44, 353-375.
- Tanabe, S., 1963: Low latitude analysis at the formative stage of typhoons in 1962. Kenkyu Jiho, 15, 405-418.
- Yanai, M., 1961: A detailed analysis of typhoon formation. Journal of Meteorological Society, Japan, 39, 187-214.
- _____, 1963: A preliminary survey of large scale disturbances over the Tropical Pacific Region. Geofisica Internacional, 3, 73-84.
- _____, 1964: An experimental objective analysis in the tropics. Atmospheric Science Paper No. 62, Colorado State University.
- Zipser, E. J., 1964: On the thermal structure of developing tropical cyclones. National Hurricane Research Project Report No. 67.